

**ALLABY Pilot Survey: the Tully Fisher Relation in Eridanus, Hydra, Norma and NGC4636 cluster field**

Hélène M. Courtois<sup>1</sup>, Jeremy Mould<sup>2</sup>, Khaled Said<sup>3</sup>, Alexandra Dupuy<sup>1</sup>, Daniel Pomarède<sup>4</sup>, Tao Hong<sup>5</sup>, Daniel Guinet<sup>1</sup>, Tobias Westmeier<sup>6</sup>, Lister Staveley Smith<sup>6</sup>, Cullan Howlett, Baerbel Koribalski<sup>6</sup>, +<sup>++6</sup>,

<sup>1</sup>*University Lyon 1, IUF, IP2I Lyon, 69622 Villeurbanne cedex, France*

<sup>2</sup>*Centre for Astrophysics & Supercomputing, Swinburne University*

<sup>3</sup>*School of Mathematics and Physics, The University of Queensland, Brisbane, QLD 4072, Australia*

<sup>4</sup>*University of Western Australia*

<sup>5</sup>*Australia Telescope National Facility*

<sup>6</sup>*IRFU, CEA Université Paris-Saclay, 91191 Gif-sur-Yvette, France*

<sup>5</sup>*National Astronomical Observatory of China*

## ABSTRACT

The Australian SKA Pathfinder network of radio-antennas is used to conduct the WALLABY phase 1 pilot survey on four fields in the direction of the heart of Laniakea supercluster. This zone is known as the Great Attractor region. Our pilot data are in the direction of Eridanus, Hydra, Norma and NGC 4636 clusters. This blind survey produced 614 galaxy spectra at 21 cm wavelength. After quality inspection 472 WALLABY spectra can be used for Tully-Fisher, however the inclination cut (only galaxy disk with  $b/a < 0.8$ ) drives this number down to 315 galaxies for which we derive a distance using W1 WISE magnitude of their optical counterpart.

*Subject headings:* s

surveys – techniques: photometric – radio astronomy: 21 cm

## 1. INTRODUCTION

Brent Tully and Richard Fisher ([Tully & Fisher 1977](#)) discovered a relation (the TFR) between the extensive properties of disk galaxies (mass, luminosity and radius) and the velocity width of their neutral hydrogen 21 cm spectra, a measure of their rotation velocity. If galaxy surface brightness, stellar mass and its mass to light ratio are functions of halo mass, the virial theorem leads one to expect a luminosity, rotation velocity relation. The TFR can be used to measure galaxy distances and peculiar velocities. The TFR can also be used to probe galaxy formation, as a TFR is seen in dark matter simulations, when sub-grid physics is added to follow the baryons (e.g. ([Springel et al. 2018](#))). Developments in understanding galaxy scaling relations are reviewed by ([Mould 2020](#)).

The Widefield ASKAP L-band Legacy All-sky Blind Survey (WALLABY) pilot survey is a study of four fields with the ASKAP telescope and is a precursor to the WALLABY survey, a blind neutral hydrogen survey of the Southern two-thirds of the sphere ([Koribalski et al. 2020](#)). In this paper we explore the infrared TFR, using Data Releases from application of the standard survey software to data acquired with the standard survey parameters. Infrared wavelengths have the advantage of markedly lower extinction of galaxy radiation by dust ([Aaronson et al. 1979](#)).

In this paper we describe the pilot survey and present optical identifications of the sources detected at 21 cm (§2); we form TFRs in the WISE W1 photometric bandpasses (§3); and we study the intrinsic scatter of the TFR which is important, because of distance biases, to its use to measure cosmic flows. Finally, we show how the WALLABY Survey can add to the Cosmic Flows database for the study of large scale structure.

## 2. WALLABY pilot survey

WALLABY is a survey with the ASKAP telescope,  $36 \times 12\text{-m}$  dishes with baselines of length 22m to  $\sim 2$  km. The detectors are phased array feeds (chequerboard) with a beam size of  $\sim 30$  sq deg and a resolution of  $\sim 30$  arcsec. The bandwidth is 1130 – 1430 MHz, –2000 to +77,000 km/s. Resolution of the spectra is  $\sim 4$  km/s per pixel. Sensitivity is  $\sim 0.7$  mJy/beam.

## 2.1. Observations and data reduction

The pilot survey uses the spectra of galaxies in Eridanus super-group, Hydra DR2, Norma DR1 and NGC4636 clusters from SoFiA ([Serra et al. 2015](#)). Detections were linked across a spatial and spectral radius of 2 with a minimum size requirement for reliable source of 5 spatial pixels and 8 spectral channels. SoFiA’s reliability filter was then applied to remove all detections with a reliability below 0.8, using a Gaussian kernel density estimator of size 0.35 times the covariance. All remaining sources were then parameterised, assuming a restoring beam size of  $\approx 30''$  for all integrated flux measurements.

The precursor Eridanus super group field was observed twice with the same center but rotated by 45 degrees. Norma, Hydra and NGC4636 pilot surveys were conducted with two adjacent on the sky and overlapping tiles (1 and 2) re-observed with a rotation (A and B) each of 5.4 degrees in side. This gives eight pointings per cluster field exposed for eight hours. Each HI spectrum is thus an integration of 16 hours. The centers of the tiles are :

Tile	J2000 coordinates of the center	
Eridanus super group	03:38:00	-22:30:00
Hydra-1A	10:15:47.844	-27:22:27.66
Hydra-1B	10:17:49.958	-27:49:24.30
Hydra-2A	10:39:24.238	-27:22:27.66
Hydra-2B	10:41:26.352	-27:49:24.30
NGC4636-1A	12:38:02.328	-00:26:59.95
NGC4636-1B	12:39:50.337	-00:53:59.85
NGC4636-2A	12:38:02.729	+04:56:58.64
NGC4636-2B	12:39:51.059	+04:29:58.13
Norma-1A	16:16:30.928	-59:27:41.88
Norma-1B	16:20:06.332	-59:54:30.90
Norma-2A	16:55:26.063	-59:27:41.88
Norma-2B	16:59:01.467	-59:54:30.90

## 2.2. Velocity widths

Following the Cosmicflows program, we measure the neutral hydrogen linewidth at 21cm wavelength enclosing 50% of the cumulative HI line flux,  $W_{m50}$  ([Courtois et al. 2011a](#)) ([Courtois et al. 2011b](#)). This parameter,  $W_{m50}$ , is the line width measured at the flux level that is 50%

of the mean flux, averaged in channels within the wavelength range enclosing 90% of the total integrated flux. However, the parameter  $W_{\text{m}50}$  is only an empirical measure of the true width of an HI galaxy velocity profile. A correction for redshift and instrumental broadening was applied:  $W_{\text{m}50}^c = \frac{W_{\text{m}50}}{1+z} - 2\Delta v \lambda$ , where  $z$  is the redshift,  $\Delta v$  is the smoothed spectral resolution, and  $\lambda = 0.25$  is an empirically determined constant. The observed line width was also adjusted by separating out the broadening from turbulent motions and offsets to produce an approximation to  $2V_{\text{max}}$ , where  $V_{\text{max}} = w_{50}(0)/2$  characterizes the rotation rate over the main body of a galaxy. (Tully & Fouque 1985) define the parameter  $W_{\text{mx}}$  as:

$$W_{\text{mx}}^2 = W_{\text{m}50}^2 + W_{\text{t,m}50}^2 \left[ 1 - 2e^{-(W_{\text{m}50}/W_{\text{c,m}50})^2} \right] - 2W_{\text{m}50}W_{\text{t,m}50} \left[ 1 - e^{-(W_{\text{m}50}/W_{\text{c,m}50})^2} \right]. \quad (1)$$

The parameters  $W_{\text{c,m}50} = 100$  km/s and  $W_{\text{t,m}50} = 9$  km/s are set after tests conducted in (Courtois et al. 2009), and characterize respectively the transition from boxcar to Gaussian intrinsic profiles, and the turbulent broadening for the observed line width considered. It is then related to the rotation rate  $V_{\text{max}}$  by:

$$w_{50}(0) = \frac{W_{\text{mx}}}{\sin(i)}, \quad (2)$$

where  $i$  is the inclination of the galaxy from face-on relative to the observer.

Details regarding the  $W_{\text{m}50}$  and  $W_{\text{mx}}$  line width parameters and comparisons with alternatives are discussed in (Courtois et al. 2009). These values replace the line widths supplied in the pilot survey data release (see Figure 1).

We have used two algorithms to calculate the 50% width from the spectra, and these are compared in 2. The widths differ by  $7.9 \pm 0.8$  km/s. We adopt that used by the Cosmicflows collaboration, which has been corrected following equation (1).

The second algorithm that we are using here is adopted from Said et al. (2016) hereafter S16. This algorithm requires prior knowledge of the left and right horns and returns the linewidth measured at 50% of the mean flux and their associated uncertainty measured through MC error estimation. In addition, this algorithm returns linewidth measurements at 20% and 50% of the peak flux, 50% of the peak flux measured from a straight-line fit to both sides of the profile, and 50% of the peak flux measured at each of the two peaks along with their associated MC errors. In this paper, we are only using the linewidth measured at 50% of the mean flux. However, the other measurements of the linewidth might be of interest to other groups.

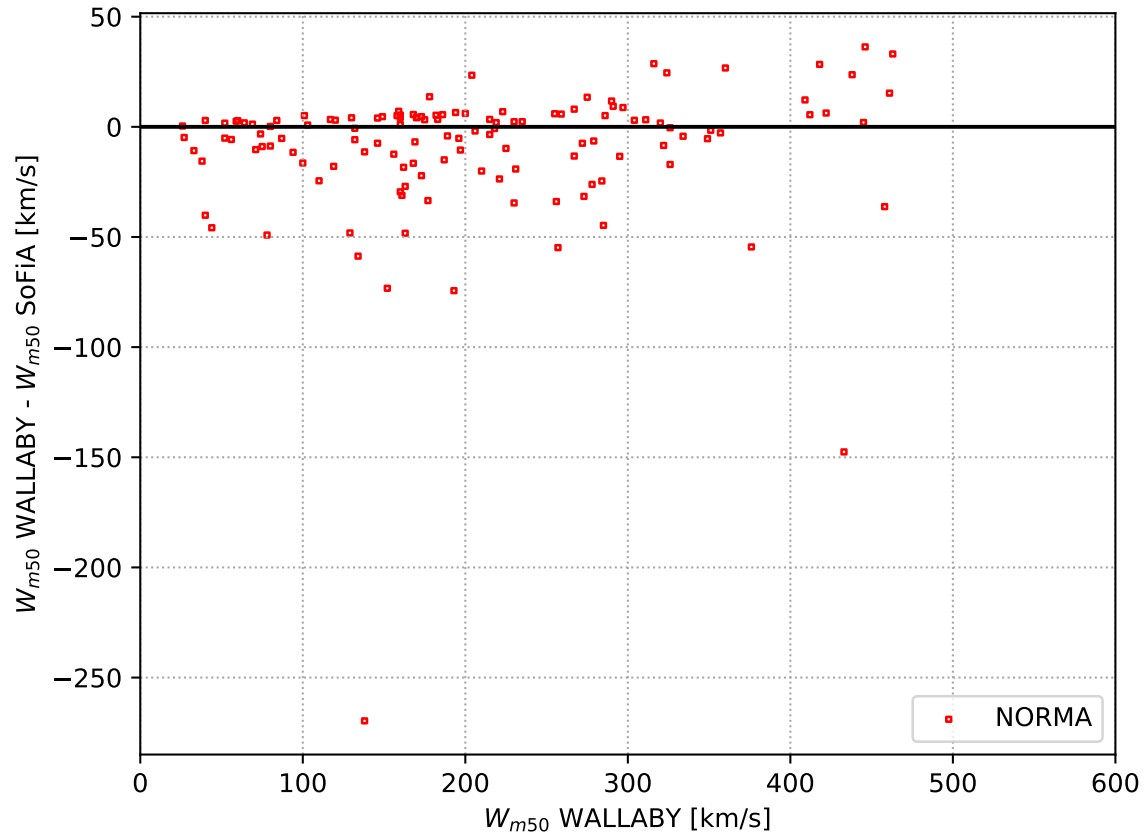


Fig. 1.— Linewidths  $W_{m50}$  in the Norma field as measured by the CosmicFlows algorithm correlates well with the automatic measurements made by the SOFiA code. The plot is for galaxies with error on  $W_{m50}$  less or equal to 20km/s.

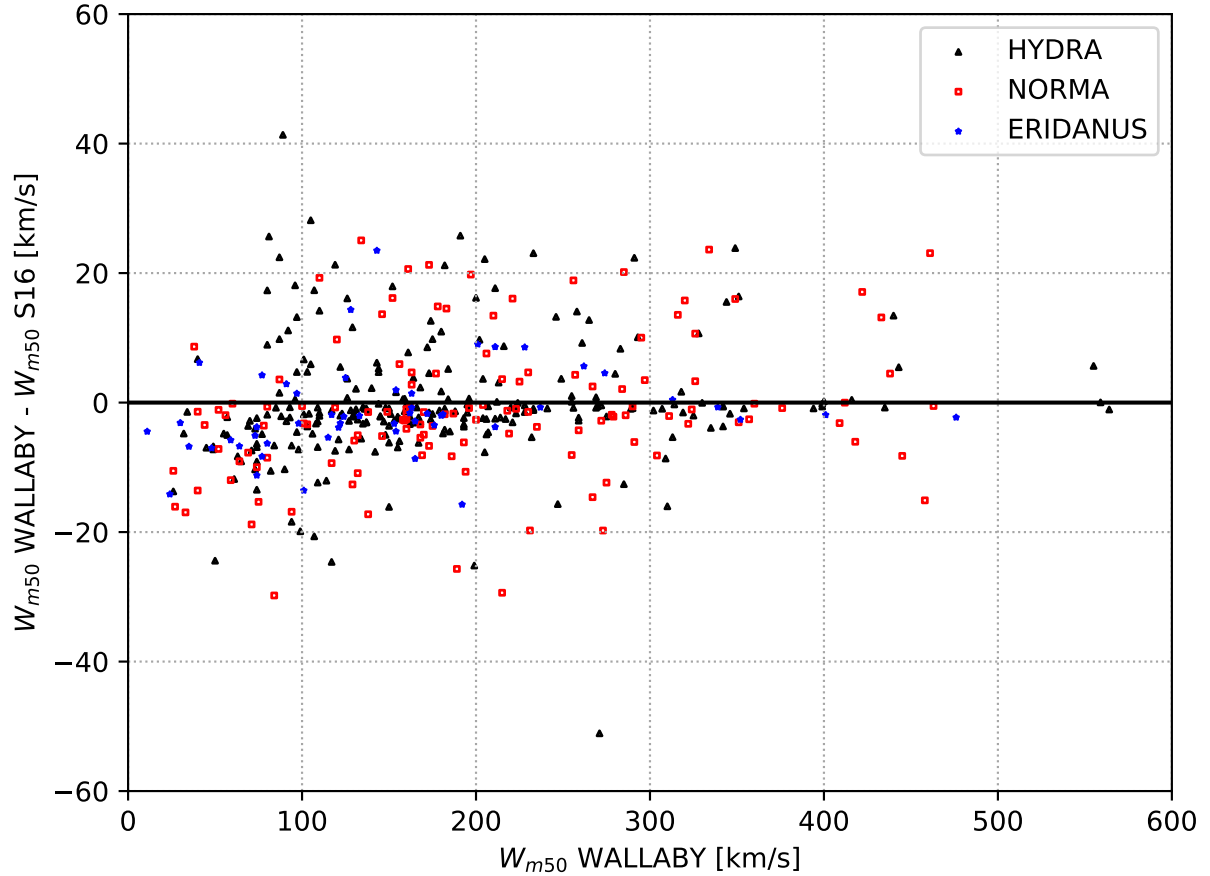


Fig. 2.— Comparison of 50% linewidths measured with the Cosmicflows algorithm and linewidths measured at 50% of the mean flux from the S16 algorithm Said et al. (2016). Only spectra providing an adequate quality are displayed (error on  $W_{m50}$  less or equal to 20 km/s).

We used the relative error between pairs of measurements to quantitatively check for any large discrepancies between 50% widths measured with the Cosmicflows algorithm and widths measured at 50% of the mean flux from the S16 algorithm. We used the pairwise relative error of the form

$$\epsilon = \frac{WM50_{CF} - WM50_{S16}}{\sqrt{(eWM50_{CF}^2 + eWM50_{S16}^2)}} \quad (3)$$

where  $WM50_{CF}$ ,  $WM50_{S16}$ ,  $eWM50_{CF}$ , and  $eWM50_{S16}$  are the 50% widths measurements from Cosmicflows and S16 algorithms and their associated errors, respectively. Although,  $\epsilon$  for all galaxies are within the distribution of a Gaussian with a mean of zero and a standard deviation of unity, Table 1 lists all galaxies with  $|\epsilon| > 1.0$ .

Following the Cosmicflows collaboration, the signal to noise (SNR) is derived as the ratio of the signal at 50% of the mean flux, over the noise measured beyond the extremities of the signal (Courtois & Tully 2015).

The error on the linewidth,  $e_W$ , is given by (Courtois et al. 2009):

$$\begin{aligned} \text{SNR} \geq 17 \quad e_W &= 8; \\ 2 < \text{SNR} < 17 \quad e_W &= 21.6 - 0.8 \text{ SNR}; \\ \text{SNR} \leq 2 \quad e_W &= 70 - 25 \text{ SNR}, \end{aligned} \quad (4)$$

where SNR is signal-to-noise ratio. An HI target is considered adequate for estimating its distance through the TFR, if its error on  $W_{m50}$  is less or equal to 20 km/s.

This gives us three algorithms for Wm50 : SOFIA is automated but sometimes gives wrong measurements (as seen in Figure 1) and with a dispersion of about 50 km/s, which is too high for Tully-Fisher purposes. The adopted code is semi-automatic : with a final inspection by eye on the fit of the line, however in some cases I was unable at all to fit the spectrum. This happened in 10% of the cases of the pilot survey: 6 spectra. The S16 code requires a starting value for Wm50 (that can be provided by the adopted code and/or Sofia's code). S16 and the adopted code agree within the 20 km/s limit on Wm50, that we impose for Tully-Fisher work.

This comparison of 3 algorithms for the measurement of Wm50 as seen in Figures 1 and 2, show how robust the three algorithms are. They agree within the error threshold we impose for deriving Tully-Fisher distances for galaxies of 20 km/s. In the rest of the article, we will be using the Wm50 values of CosmicFlows algorithm apart from a few galaxies that were best fitted by the S16 algorithm.

All the galaxy 21 cm spectra that were finally selected for this TF study are displayed in Table 2.

### 2.3. Optical identifications

The photometric data are obtained from the Wide-field Infrared Survey Explorer (WISE, Wright et al. 2010) All-Sky source catalog. WISE mapped the whole sky in four bands W1, W2, W3 and W4 centered at 3.4, 4.6, 12 and 22  $\mu\text{m}$ , and provides more than 563 million measurements of infrared sources. The photometric quantities adopted in this paper are the instrumental profile-fit magnitudes and their uncertainties in the W1 band. The WALLABY spectrum sample was cross-matched with the WISE All-Sky source catalog using a search radius of 30 arcsec, which corresponds with the spatial resolution of WALLABY pilot survey.

As for the disk inclination correction needed to de-project the HI linewidth, we have used inclinations for all the galaxies provided by [SkyMapper data server](#).

The pilot survey uses for the first time multi-dish radio-telescopes for Tully-Fisher purpose, thus it is important to compare these new velocity widths with those previously measured using single dish spectroscopy. Galaxy cross-identification is also an external test of the robustness of matching optical counterparts to WALLABY spectra. As shown in Figure 3) there is no significant difference when comparing the  $W_{mx}$  values. This is an excellent assessment of WALLABY instrumental capacity to deliver satisfactory datasets to the community.

## 3. Tully Fisher Relations in the four WALLABY pilot fields

In this section we compute Tully-Fisher galaxy distances using SkyMapper disk inclination information, and Wise W1 band apparent magnitude with Schlegel et al. (1998) extinction correction and a same k-correction for all galaxy types that follow a linear form  $A_{W1}^k = -2.27z$  (Oke & Sandage 1968; Huang et al. 2007). Finally we check consistency with and apply the Tully-Fisher relation calibration from Kourkchi et al. (2020a).

Disk inclination  $i$  is derived from optical photometry from SkyMapper DR3 (Keller et al. 2007; Onken et al. 2019; [SkyMapper-DR3 2020](#)) object elongation (a/b) via

$$\cos^2 i = \frac{(b/a)^2 - q_0^2}{1 - q_0^2} \quad (5)$$

where  $q_0$  is the intrinsic axial ratio of the galaxy ( $q_0 = 0.13$  for Sbc and Sc, and  $q_0 = 0.2$  for other types). We didn't make a search for the morphological type, so we used  $q_0 = 0.2$  if  $b/a > 0.2$  and  $q_0 = 0.13$  if  $b/a \leq 0.2$ .

Galaxies with inclinations less than 45° are excluded. Corrections to the W1 magnitudes

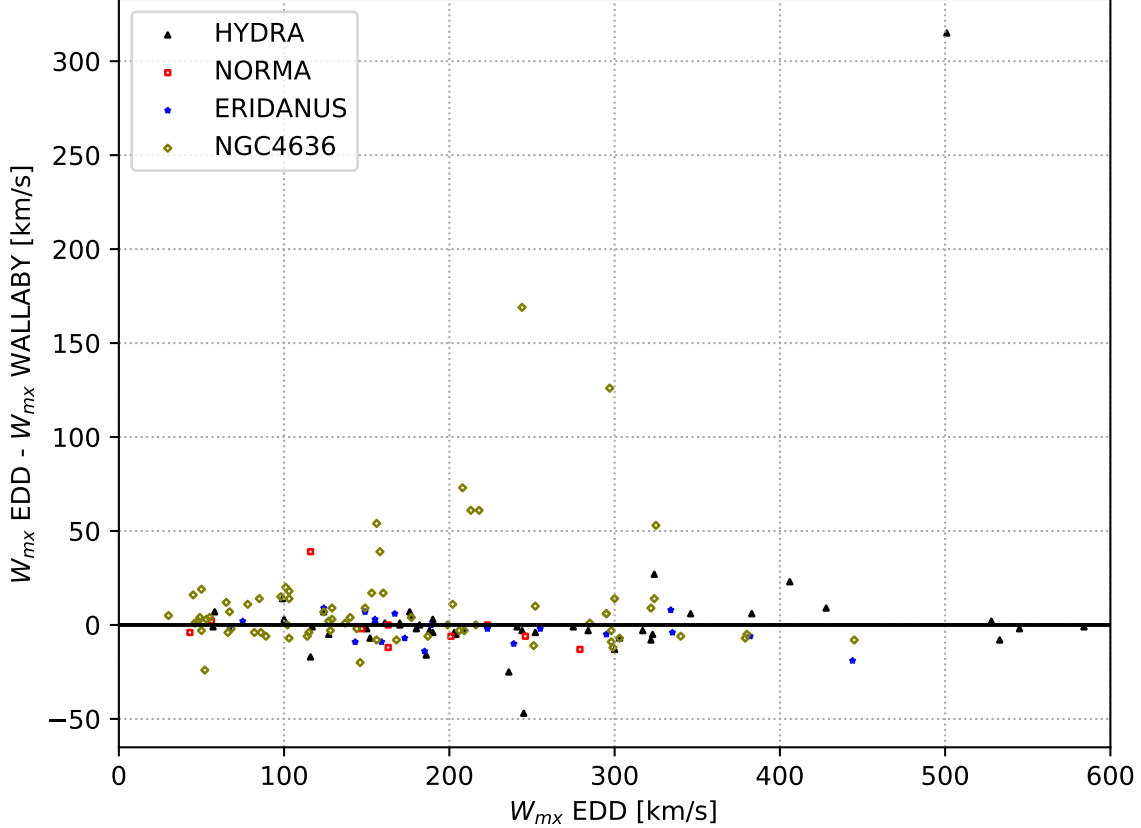


Fig. 3.— Comparison of the WALLABY pilot phase velocity widths presented in this article with the ones in the Extragalactic Distance Database ([Courtois & Tully 2015](#)). Only spectra providing an adequate quality are displayed (error on  $W_{m50}$  less or equal to 20 km/s).

for internal extinction were considered and neglected. ([Sakai et al. 2000](#)) parameterize them as  $\gamma \log a/b$ . If the effective wavelength of W1 is  $3.4\mu$ , and the absorption in magnitudes is proportional to  $\lambda^{-1}$ , its maximum value is less than 0.1 W1 magnitudes at  $\log w = 2.5$ .

Figure 5 gives an illustration of the fact that WALLABY pilot survey observe pencil beams: in the same field we observe both the front cluster galaxies and some distant galaxies.

### 3.1. The Hydra field

The Hydra cluster has a mean redshift of 0.012 ([Babyk & Vavilova 2013](#)) and a velocity dispersion of 690 km/s ([Lima-Dias et al. 2021](#)). Figure 5 shows the redshift distribution for

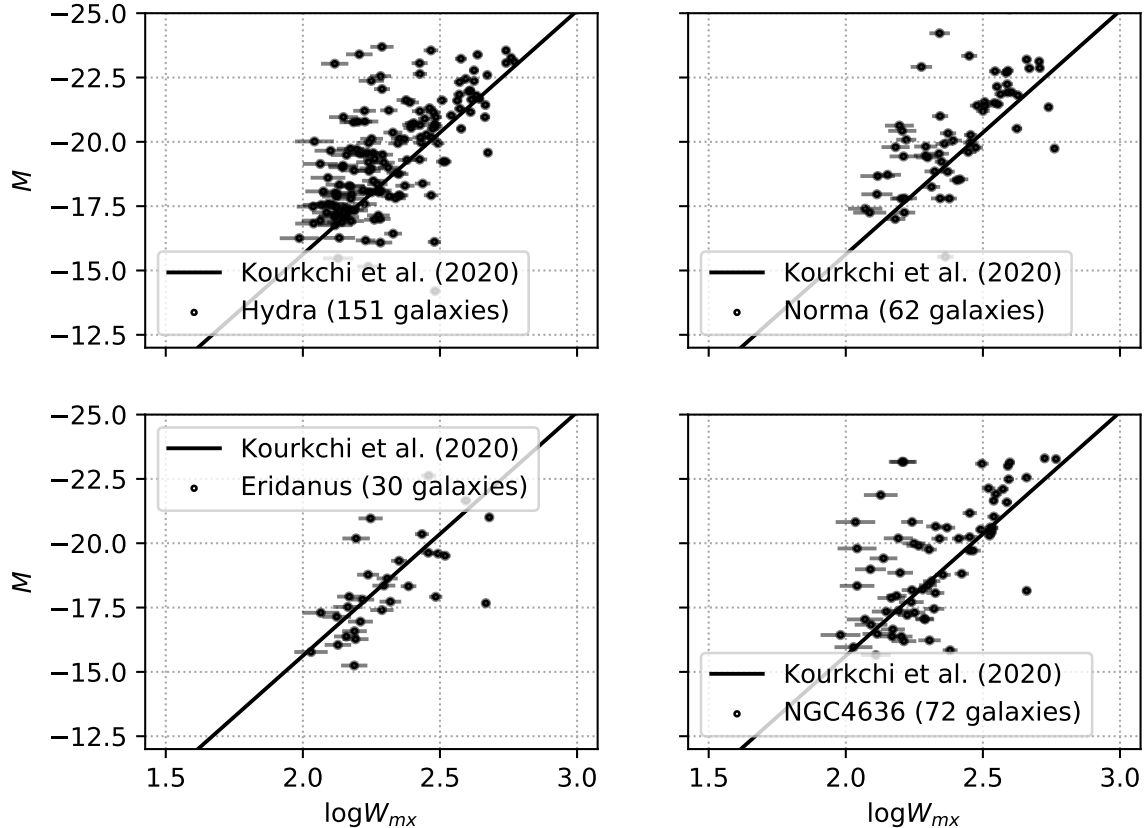


Fig. 4.— TFR for Hydra, Norma, Eridanus, and NGC4636 fields galaxies in the WISE  $W1$  band. The quantities derived with the Pilot survey are in good agreement with the WISE  $W1$  TFR calibration in [Kourkchi et al. \(2020b\)](#) (solid black line).

Hydra cluster galaxies in our sample with velocities in column (2) of Table 1 between 1700 and 6000 km/sec. Figure 6 shows the TFR distances. Corrections to the velocity widths in Figure ?? (but not Table 1) include the  $(1+z)$  cosmological term. The straight line in the figure is a fit to the data with the slope (10.05) measured by ([Lagattuta et al. 2013](#)). A 3D view of the Hydra cluster is presented by ([Courtois et al. 2012](#)).

### 3.2. The Norma field

([Woudt et al. 2008a](#)) find a mean velocity of  $4871 \pm 54$  km/s for the Norma cluster and locate its centre at  $(l, b) = (325^\circ.3, -7^\circ.2)$ . They identify it as the richest cluster in the region

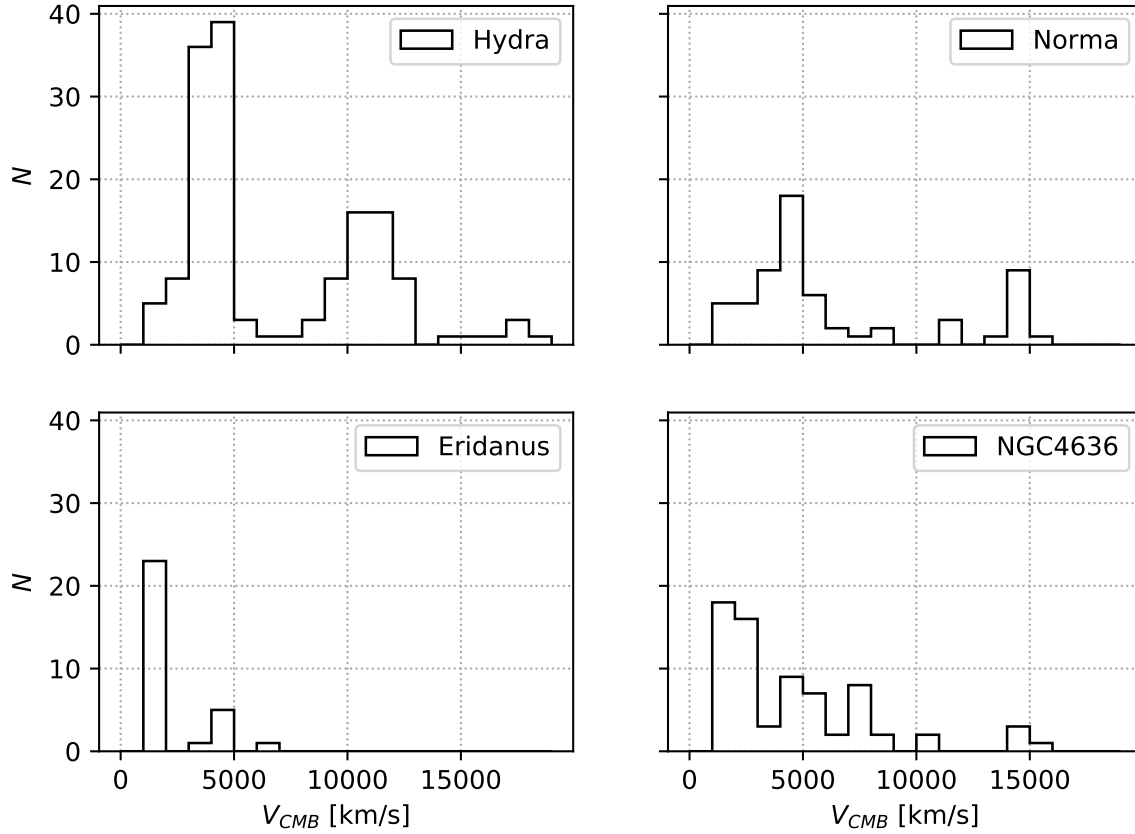


Fig. 5.— Redshift distribution of the galaxies in Hydra, Norma, Eridanus, and NGC4636 fields in the CMB frame. WALLABY pilot integration time reaches out to galaxies located at 15,000 km/s in redshift.

of the Great Attractor. (Mutabazi 2021), in a study of its fundamental plane, finds a small peculiar velocity. The WALLABY pilot survey field is centred on  $(l, b) = (329^\circ.3, -10^\circ.4)$ , *i.e.*  $5.1^\circ$  and 6 Mpc from the cluster. Nevertheless, there is an overdensity of galaxies with the cluster’s redshift (Figure 6).

We therefore plot TFR distances for the absolute magnitude of high signal to noise ( $S/N > 5$ ), low velocity width error ( $w_{50}/\delta w_{50} > 5$  galaxies in Figure 6.

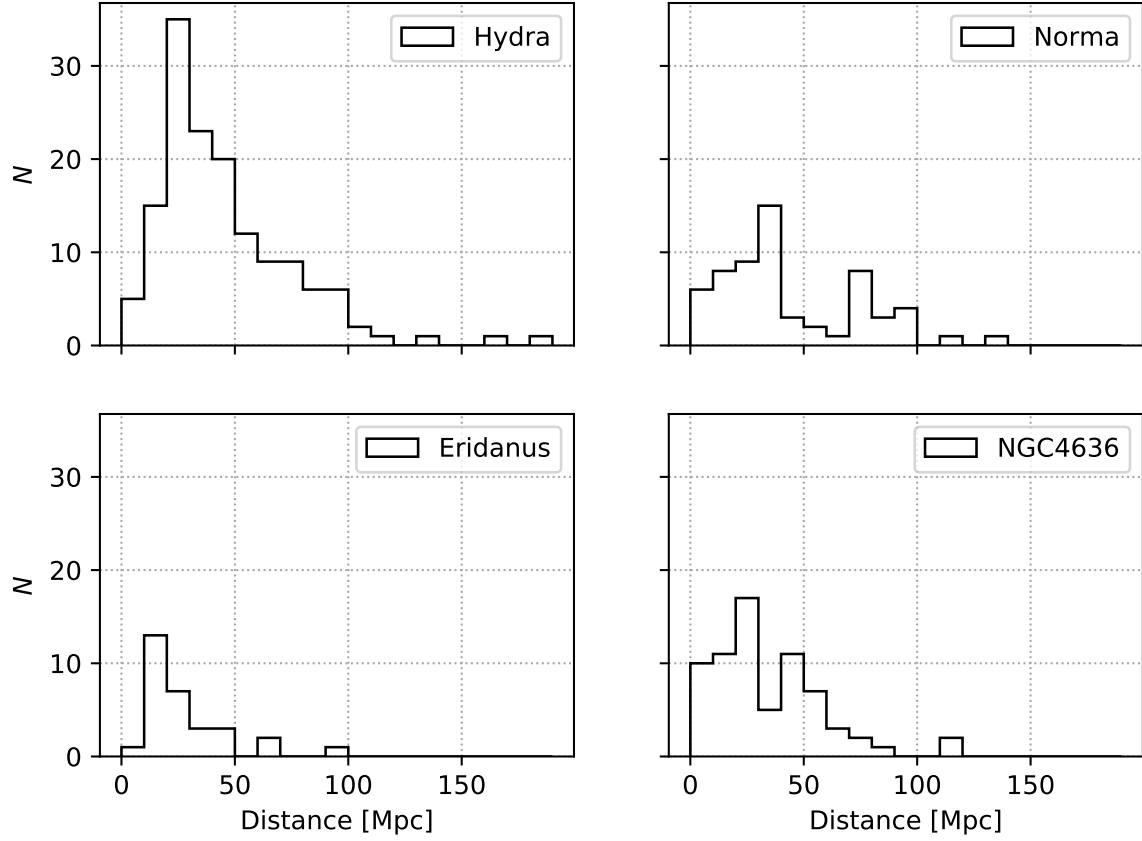


Fig. 6.— TFR distance distribution of galaxies in Hydra, Norma, Eridanus, and NGC4636 fields.

### 3.3. Scatter in the pilot survey TFR

For Jeremy to edit :

The average uncertainty in  $\log w_{50}$  in the Hydra cluster is 0.05 dex, which corresponds to 0.5 mag in the TFR for a slope of 10.05. The average uncertainty in  $W_1$  is 0.05 mag. Galaxies catalogued by (Lauberts 1982) scatter in  $b/a$  by 0.1 rms relative to the measurements made here. Over the range  $45^\circ < i < 90^\circ$  this corresponds to 0.9 to 0.3 mag when multiplied by the slope of the TFR. We summarize these contributions to the Hydra and Norma TFR magnitude scatter in the table.

#### 4. Spatial distribution of galaxies in the Pilot Survey

Infall to the Norma cluster takes the form of a sharper distribution in redshift space than in real space (Figure 6). The positions of WALLABY galaxies within the Cosmic Web are studied using the density contrast  $\delta$  reconstructed from the Cosmicflows-3 Catalog of peculiar velocities (Graziani et al. 2019; Tully et al. 2019; Courtois et al. 2019; Pomarède et al. 2020). In Figure 7 are shown the locations of galaxies of the Norma survey versus a three-dimensional visualization of the overdensity field, restricted to a slice. The visualization is obtained by a combination of a ray-casting algorithm (Pomarède et al. 2017a) resulting in a smooth rendering of the  $\delta$  field ranging from most underdense (deep blue color) to most overdense (yellow), and a series of semi-transparent isosurface polygons resulting in a sharp materialization of the surfaces ranging from  $\delta = 0$  (grey surface) to highly overdense ( $\delta = 2.8$  in red). The grey surface hence marks the frontier between the underdense universe and the overdense universe. The most noticeable feature in the distribution of WALLABY galaxies is their aggregation near the Norma cluster at  $\text{SGX} \simeq -5000$  km/s, seen as a pronounced local maximum in the  $\delta$  field. Between the Local Group and the Norma cluster, the beam runs first through a section of the Local Void (Tully et al. 2019) and then through the termination of a filament connecting the Fornax cluster to the Norma cluster, as can better be seen from the interactive 3D visualization supplementing Figure 7 (see annotations 2 and 3). Beyond its intersection with the Norma-Pavo-Indus filament (Fairall 1998; Courtois et al. 2013), the beam enters in the void separating this filament and the South Pole Wall (Pomarède et al. 2020). The map of Figure 7 indicates the location of local extrema of the  $\delta$  field, such as the Ara-10.5 Void and the Ara+14.5 overdensity, for which names are conveniently given the name of the constellation in which they sit, followed by a + for an overdensity or a - for an underdensity, followed by their redshift in units of 1000 km/s, a convention established in (Tully et al. 2019). An aggregation of WALLABY galaxies is found at the location of the Ara+14.5 knot of the Cosmic Web, that is nearly coincident with the CIZA J1653.0-5943 cluster (Ebeling et al. 2002). Beyond this most distant section of the South Pole Wall, the beam presumably enters a new void, in regions where the Cosmicflows-3 reconstruction tends to null field by lack of sufficient data constraints. The most distant galaxy in the Norma beam, located at redshift 0.073, is indicated in the map.

In Figure 8 is plotted in a similar way the distribution of the WALLABY galaxies of the Hydra survey against the cosmography. The density of WALLABY galaxies as a function of distance displays contrasted features: after displaying a handful of galaxies located in our vicinity at  $\simeq 900$  km/s, the beam runs empty through the void located in the foreground of the Hydra cluster, then a major aggregation of objects is seen at the crossing of the Hydra cluster, that is part of a high-density node of the Cosmic Web, as seen in the map of the Cosmicflows-3 density contrast. In the background of the Hydra cluster, the beam enters

a deep void (Hydra-7.4) where only a very few galaxies reside. In the background of this void, the beam displays an extended cloud of galaxies scattered throughout a wall located in Hydra at about 10,000 km/s, where are found the local maxima in density: Hydra+9.7, Hydra+9.9, Antlia+8.8. After falling down as a function of distance, the number density of galaxy rises again at the most extreme distances, with WALLABY\_J104910-282305 being the most remote one at  $\sim 23,000$  km/s. This infall pattern of peculiar velocities leads to a higher overdensity in redshift space (Figure 5) than in real space (Figure 6).

The spatial distribution of the galaxies of the NGC 4636 survey is shown in Figure 9. The beam presents its highest density at the crossing of the Virgo Strand (Courtois et al. 2013), a section of the Cen-Vir-PP filament that connects the Centaurus and Perseus nodes of the Cosmic Web through the Virgo cluster (Pomarède et al. 2017b), a filament in which is nested the NGC 4636 cluster. The beam then progresses on the outskirts of the void located between Virgo and the Great Wall (Gregory & Thompson 1978), and through the Centaurus-Coma filament (Pomarède et al. 2017b). The number of galaxies then rises at the intersection of the Great Wall (de Lapparent et al. 1986) near the Virgo+6.3 and Virgo+7.1 local maxima of the density contrast. In the background of the Great Wall, the beam runs through the trough and peak of Virgo-10.3 and Virgo+14.5.

Finally, the location of the galaxies of the Eridanus super group survey is presented in Figure 10. It shows that the galaxies are found nearby the Fornax node of the Cosmic Web, and distributed along the density gradient seen in the transition toward the Sculptor Void located in the background (Pellegrini et al. 1990; Fairall 1998).

As a conclusion, it can be noticed from this series of cosmographic map, that the WALLABY survey beams are probing a vast diversity of elements of the cosmic web, intersecting numerous features such as voids, filaments, walls, and nodes. The inclusion of these galaxy tracers in future catalogues, such as in the Cosmicflows collection, will add precious data constraints for the cosmographers. Of particular interest are the regions of Hydra and Norma clusters and their roles in the dynamical structure and influence of the Great Attractor (Dressler et al. 1987; Woudt et al. 2008b; Tully et al. 2014; Hoffman et al. 2017). Of great interest are also galaxies found to reside in voids, that will provide improved constraints on the flows evacuating these underdense patches (Tully et al. 2008; Rizzi et al. 2017; Shaya et al. 2017) The most distant sections of the pencil beams, with velocities out to 22,000 km/s, will bring in new useful information on the architecture of the Cosmic Web at these remote locations.

Table 1: All galaxies with pair wise relative error  $|\epsilon| > 1.0$  between the Cosmicflows and S16 algorithms.

name	PGC	$W_{m50}$	$e_{Wm50}$	$W_{m50}^{S16}$	$e_{Wm50}^{S16}$	$\epsilon$
J102439-244547	30532	94	18	112	2	-1.0177
J102447-264054	30545	271	17	322	13	-2.4078
J103442-283406	31296	247	15	263	4	-1.0149
J103726-261843	31557	199	18	224	2	-1.3854
J104127-275119	31842	99	19	119	5	-1.0091
J104142-284653	31855	107	15	128	7	-1.2566
J104513-262755		50	17	74	6	-1.3571
J104905-292232	32361	117	17	142	3	-1.4259
J163452-603705	58536	189	17	215	1	-1.5087
J164359-600237		215	18	244	17	-1.1702
J165105-585918	59112	84	14	114	3	-2.0721
J165145-590915		71	18	90	5	-1.0111

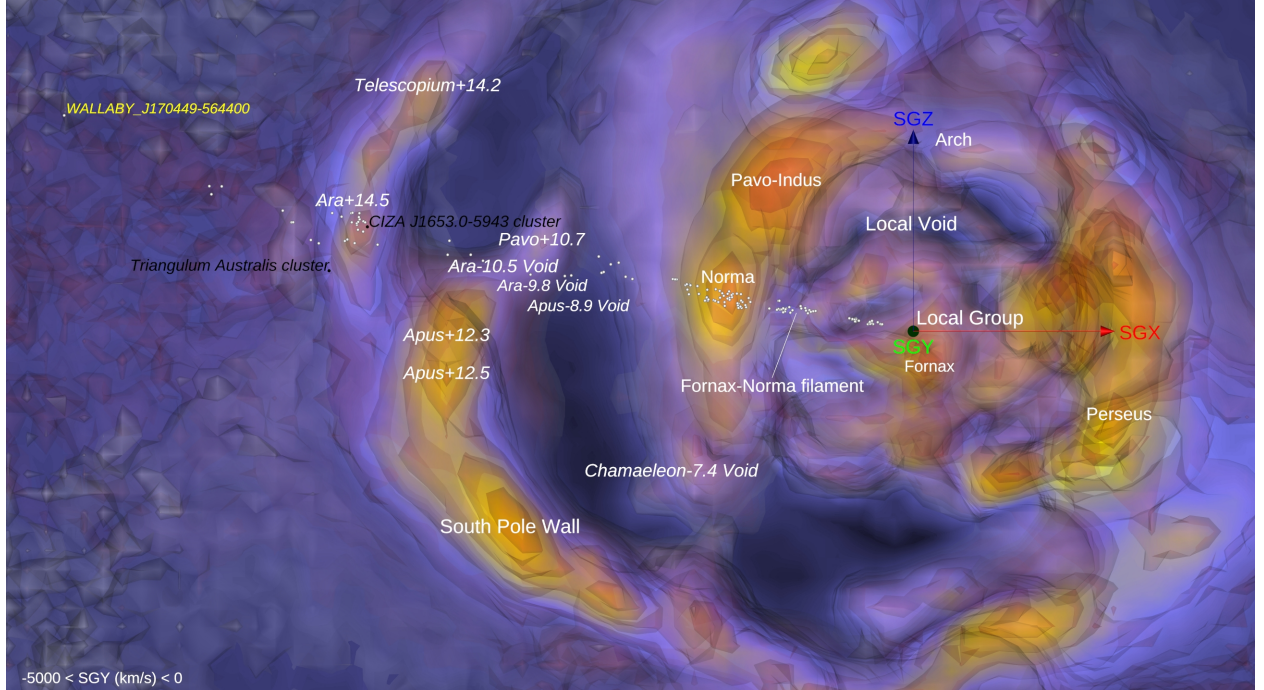


Fig. 7.— Map of the positions of galaxies in the Norma field versus the density contrast  $\delta$  as reconstructed from the Cosmicflows-3 Catalog of peculiar velocities. Scale and orientation are provided by the red, green, blue 5000 km/s-long arrows emanating from our position and associated with the three cardinal axes of the supergalactic coordinate system SGX, SGY, and SGZ, respectively. A slice contained within the SGY=-5000 km/s and SGY=0 planes is here seen from the negative SGY direction. This static view is complemented by an online [interactive 3D visualization of the Norma survey beam](#) showing three overdense levels of the  $\delta$  field. This tool can be used to better grasp how the beam runs through a sequence of voids and overdensities.

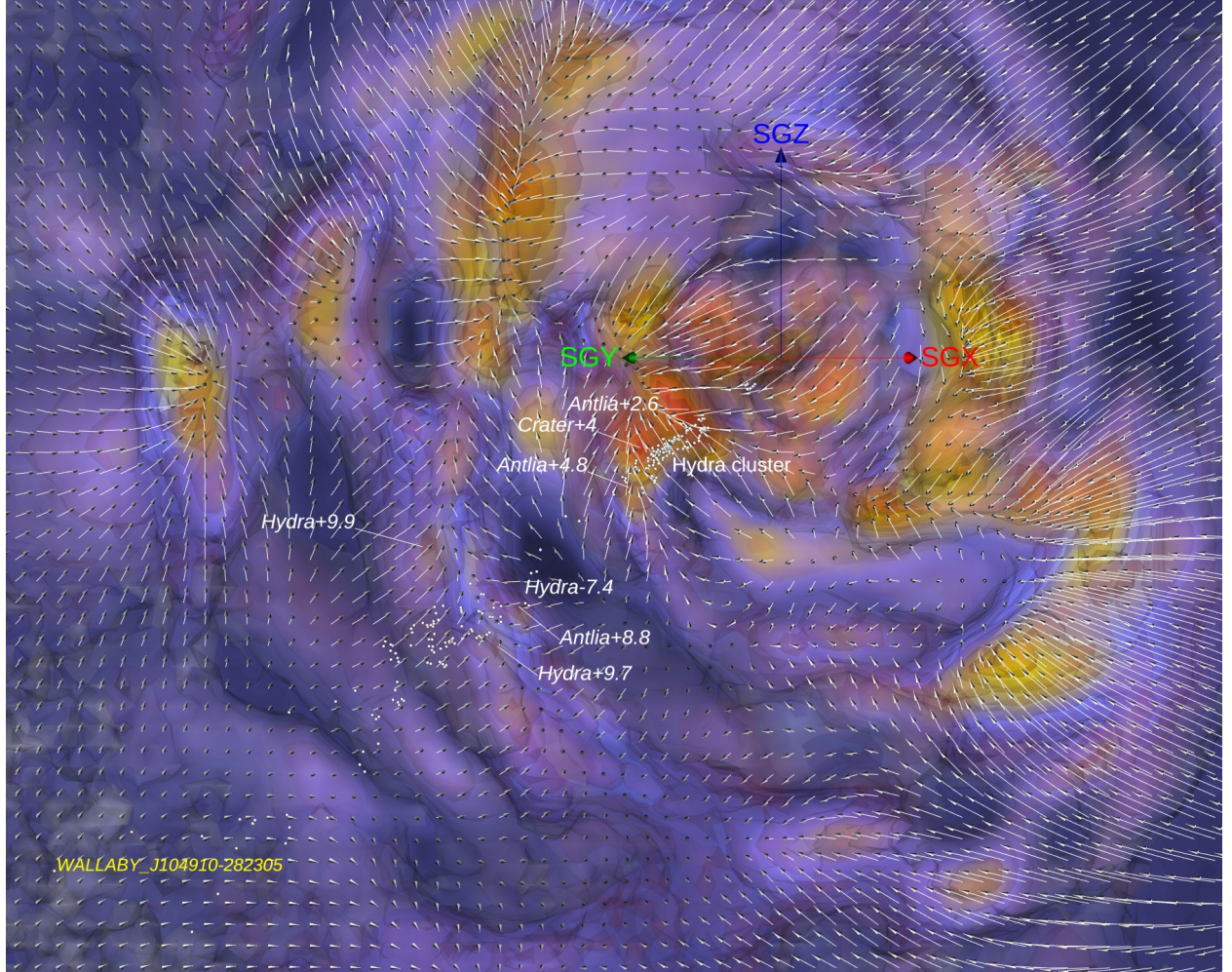


Fig. 8.— Map of the positions of galaxies in the Hydra field versus the full matter (dark + luminous) density contrast  $\delta$  field and the peculiar (gravitational) velocity field (white arrows) as reconstructed from the Cosmicflows-3 Catalog. Scale and orientation are provided by the red, green, blue 5000 km/s-long arrows emanating from our position and associated with the three cardinal axes of the supergalactic coordinate system SGX, SGY, and SGZ, respectively. A slice of 5000 km/s-thickness centered on the plane defined by the supergalactic longitude of the Hydra cluster ( $SGL = 139.36^\circ$ ) is here seen face-on. This static view is complemented by an online [interactive 3D visualization of the Hydra survey beam](#) showing three overdense levels of the  $\delta$  field. This tool can be used to better grasp how the beam runs through a sequence of voids and overdensities.

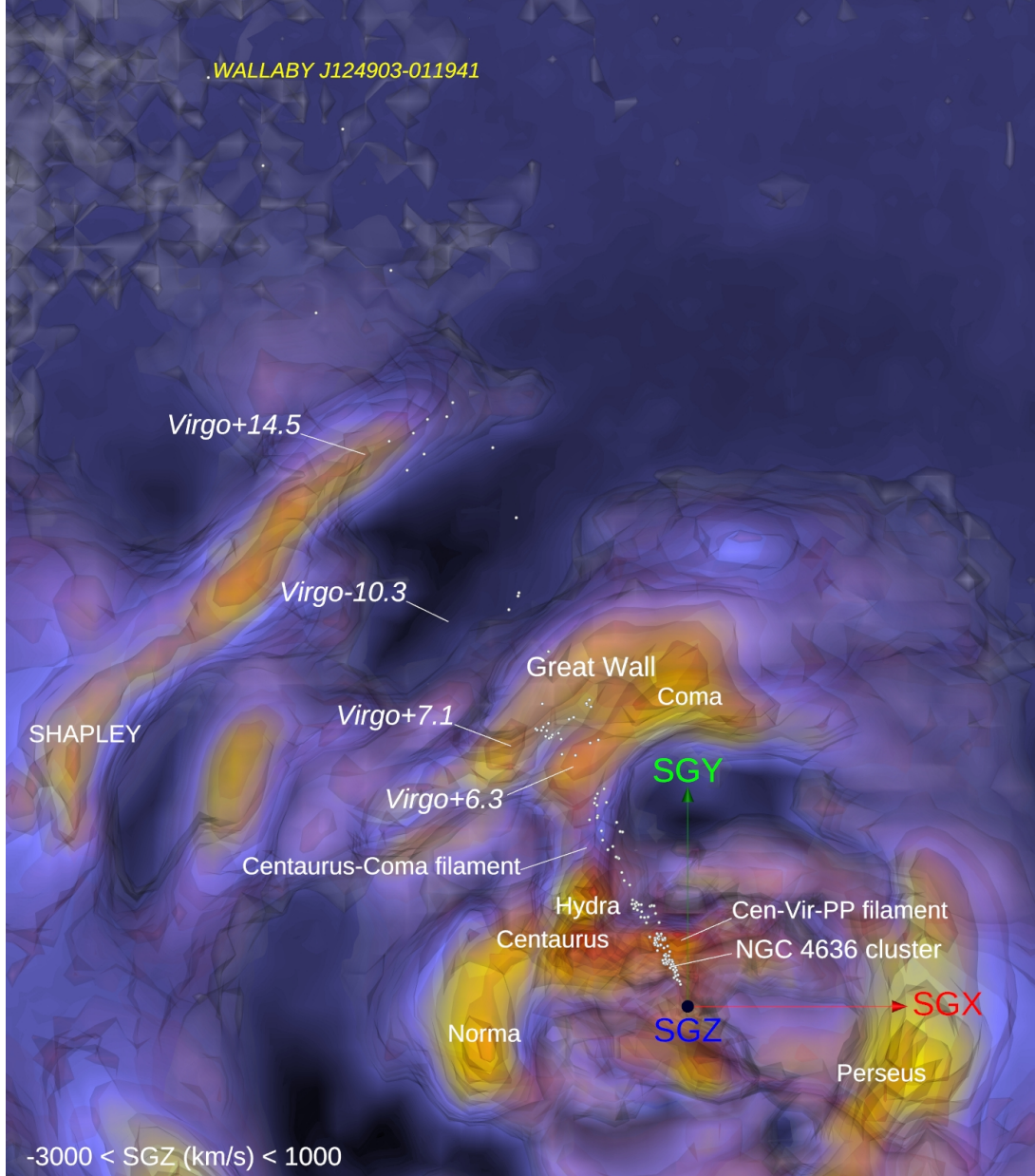


Fig. 9.— Map of the positions of galaxies in the NGC 4636 field versus the density contrast  $\delta$  as reconstructed from the Cosmicflows-3 Catalog of peculiar velocities. Scale and orientation are provided by the red, green, blue 5000 km/s-long arrows emanating from our position and associated with the three cardinal axes of the supergalactic coordinate system SGX, SGY, and SGZ, respectively. A slice contained within the SGZ = -3000 km/s and SGZ = +1000 km/s planes is here seen from the positive SGZ direction. This static view is complemented by an online [interactive 3D visualization of the NGC 4636 survey beam](#).

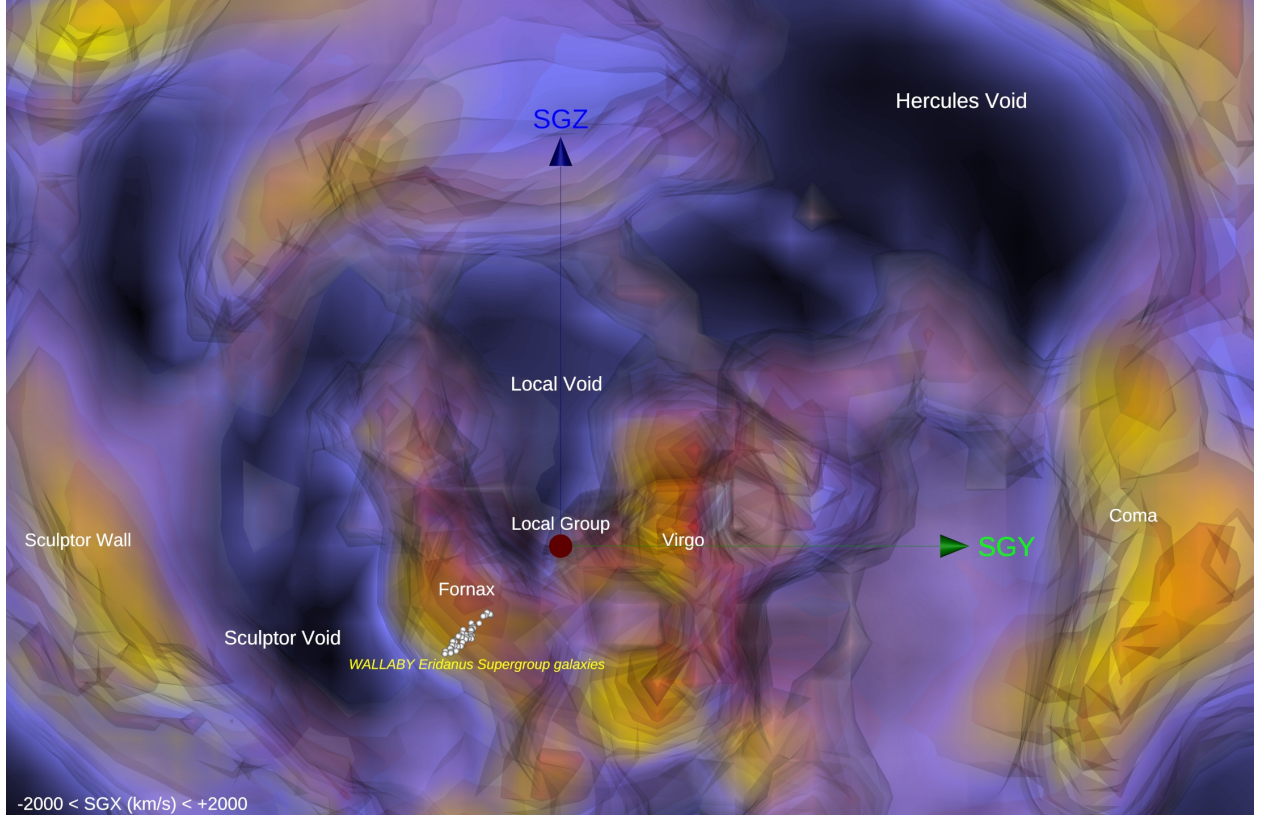


Fig. 10.— Map of the positions of galaxies in the Eridanus super group versus the density contrast  $\delta$  as reconstructed from the Cosmicflows-3 Catalog of peculiar velocities. Scale and orientation are provided by the red, green, blue 5000 km/s-long arrows emanating from our position and associated with the three cardinal axes of the supergalactic coordinate system SGX, SGY, and SGZ, respectively. A slice contained within the SGX = -2000 km/s and SGX = +2000 km/s planes is here seen from the positive SGX direction. This static view is complemented by an online [interactive 3D visualization of the Eridanus super group survey](#).

## 5. Peculiar Velocities in the region of the Great Attractor

The peculiar velocities for the Hydra and Norma fields show an infall pattern to the Hydra and Norma clusters, i.e. positive peculiar velocities on the nearside of the clusters and negative on the far side. Beyond Hydra, positive velocities return as the galaxies come under the influence of the wall located at about 10,000 km/s  $\simeq$  135 Mpc, seen in Figure 8 at the locations of the local maxima Hydra+9.7 and Hydra+9.9. The pattern observed in the peculiar velocities at  $\sim$  100 Mpc is typical of an evacuation by the void located at 7400 km/s, labelled Hydra-7.4 in Figure 8, whereby galaxies located in the foreground of this void get negative velocities, while galaxies located in the background of this void get positive velocities. The wealth of data represented by the WALLABY galaxies located along this beam at these large distances will play an important role in mapping the structure hinted by the Cosmicflows-3 reconstruction, in particular of the wall seen in Hydra at 10,000 km/s.

## 6. Conclusions

- Velocity widths measured with ASKAP are in excellent agreement with those previously measured with single dish observations
- W1 band TFRs enable investigation of peculiar velocities of galaxies in the WALLABY survey.
- Even as close to the zone of avoidance as the Norma cluster extinction in  $W1 < 0.05$  mag.
- The kinematic pattern in the Hydra and Norma fields is one of infall to the cluster mass concentrations.
- The WALLABY pilot survey sensitivity will extend investigation of peculiar velocities beyond what was previously achieved with single dish methods (TFR and Fundamental plane).
- The largest contributors to the 0.8 mag *rms* scatter of this TFR is the measurement of optical galaxy disk inclinations and the signal to noise ratio of WALLABY 21 cm spectra.

The Australian SKA Pathfinder is part of the Australia Telescope National Facility which is managed by CSIRO. Operation of ASKAP is funded by the Australian Government

with support from the National Collaborative Research Infrastructure Strategy. ASKAP uses the resources of the Pawsey Supercomputing Centre. Establishment of ASKAP, the Murchison Radio-astronomy Observatory and the Pawsey Supercomputing Centre are initiatives of the Australian Government, with support from the Government of Western Australia and the Science and Industry Endowment Fund. We acknowledge the Wajarri Yamatji people as the traditional owners of the Observatory site. We would like to thank all our colleagues on the WALLABY team for helpful discussions. We have made use of NASA data products, including WISE and NED, and also NSF OIR Lab data products.

HC is grateful to the Institut Universitaire de France and CNES for its support. AD acknowledges financial support from the Project IDEXLyon at the University of Lyon under the Investments for the Future Program (ANR-16-IDEX-0005). KS acknowledges support from the Australian Government through the Australian Research Council’s Laureate Fellowship funding scheme (project FL180100168). We acknowledge the use of the HyperLeda database. This project is partly financially supported by Region Rhône-Alpes-Auvergne. Many thanks to Dmitry Makarov for helping us on the cross-identification with galaxy PGC names.

## REFERENCES

- Aaronson, M., Huchra, J., & Mould, J. 1979, ApJ, 229, 1
- Babyk, I. V. & Vavilova, I. B. 2013, Odessa Astronomical Publications, 26, 175
- Courtois, H. M., Hoffman, Y., Tully, R. B., & Gottlöber, S. 2012, ApJ, 744, 43
- Courtois, H. M., Kraan-Korteweg, R. C., Dupuy, A., Graziani, R., & Libeskind, N. I. 2019, MNRAS, 490, L57
- Courtois, H. M., Pomarède, D., Tully, R. B., Hoffman, Y., & Courtois, D. 2013, AJ, 146, 69
- Courtois, H. M. & Tully, R. B. 2015, MNRAS, 447, 1531
- Courtois, H. M., Tully, R. B., Fisher, J. R., et al. 2009, AJ, 138, 1938
- Courtois, H. M., Tully, R. B., & Héraudeau, P. 2011a, MNRAS, 415, 1935
- Courtois, H. M., Tully, R. B., Makarov, D. I., et al. 2011b, MNRAS, 414, 2005
- de Lapparent, V., Geller, M. J., & Huchra, J. P. 1986, ApJ, 302, L1
- Dressler, A., Faber, S. M., Burstein, D., et al. 1987, ApJ, 313, L37

- Ebeling, H., Mullis, C. R., & Tully, R. B. 2002, ApJ, 580, 774
- Fairall, A. P. 1998, Large-scale structures in the universe / Anthony P. Fairall. New York : Wiley, 1998. (Wiley-Praxis series in astronomy and astrophysics)
- Graziani, R., Courtois, H. M., Lavaux, G., et al. 2019, MNRAS, 488, 5438
- Gregory, S. A. & Thompson, L. A. 1978, ApJ, 222, 784
- Hoffman, Y., Pomarède, D., Tully, R. B., & Courtois, H. M. 2017, Nature Astronomy, 1, 0036
- Huang, J. S., Ashby, M. L. N., Barmby, P., et al. 2007, ApJ, 664, 840
- Keller, S. C., Schmidt, B. P., Bessell, M. S., et al. 2007, PASA, 24, 1
- Koribalski, B. S., Staveley-Smith, L., Westmeier, T., et al. 2020, Ap&SS, 365, 118
- Kourkchi, E., Tully, R. B., Anand, G. S., et al. 2020a, ApJ, 896, 3
- Kourkchi, E., Tully, R. B., Neill, J. D., et al. 2020b, ApJ, 884, 82
- Lagattuta, D. J., Mould, J. R., Staveley-Smith, L., et al. 2013, ApJ, 771, 88
- Lauberts, A. 1982, ESO/Uppsala survey of the ESO(B) atlas
- Lima-Dias, C., Monachesi, A., Torres-Flores, S., et al. 2021, MNRAS, 500, 1323
- Mould, J. 2020, Frontiers in Astronomy and Space Sciences, 7, 21
- Mutabazi, T. 2021, ApJ, 911, 16
- Oke, J. B. & Sandage, A. 1968, ApJ, 154, 21
- Onken, C. A., Wolf, C., Bessell, M. S., et al. 2019, PASA, 36, e033
- Pellegrini, P. S., da Costa, L. N., Huchra, J. P., Latham, D. W., & Willmer, C. N. A. 1990, AJ, 99, 751
- Pomarède, D., Courtois, H. M., Hoffman, Y., & Tully, R. B. 2017a, PASP, 129, 058002
- Pomarède, D., Hoffman, Y., Courtois, H. M., & Tully, R. B. 2017b, ApJ, 845, 55
- Pomarède, D., Tully, R. B., Graziani, R., et al. 2020, ApJ, 897, 133
- Rizzi, L., Tully, R. B., Shaya, E. J., Kourkchi, E., & Karachentsev, I. D. 2017, ApJ, 835, 78

- Said, K., Kraan-Korteweg, R. C., Staveley-Smith, L., et al. 2016, MNRAS, 457, 2366
- Sakai, S., Mould, J. R., Hughes, S. M. G., et al. 2000, ApJ, 529, 698
- Schlegel, D. J., Finkbeiner, D. P., & Davis, M. 1998, ApJ, 500, 525
- Serra, P., Westmeier, T., Giese, N., et al. 2015, MNRAS, 448, 1922
- Shaya, E. J., Tully, R. B., Hoffman, Y., & Pomarède, D. 2017, ApJ, 850, 207
- SkyMapper-DR3. 2020, PASA, DOI:10.25914/5f14edcd2d116
- Springel, V., Pakmor, R., Pillepich, A., et al. 2018, MNRAS, 475, 676
- Tully, R. B., Courtois, H., Hoffman, Y., & Pomarède, D. 2014, Nature, 513, 71
- Tully, R. B. & Fisher, J. R. 1977, A&A, 54, 661
- Tully, R. B. & Fouque, P. 1985, ApJS, 58, 67
- Tully, R. B., Pomarède, D., Graziani, R., et al. 2019, ApJ, 880, 24
- Tully, R. B., Shaya, E. J., Karachentsev, I. D., et al. 2008, ApJ, 676, 184
- Woudt, P. A., Kraan-Korteweg, R. C., Lucey, J., Fairall, A. P., & Moore, S. A. W. 2008a, MNRAS, 383, 445
- Woudt, P. A., Kraan-Korteweg, R. C., Lucey, J., Fairall, A. P., & Moore, S. A. W. 2008b, MNRAS, 383, 445
- Wright, E. L., Eisenhardt, P. R. M., Mainzer, A. K., et al. 2010, AJ, 140, 1868

Table 2:: Hydra HI data from WALLABY phase 1 pilot survey

name	PGC	ra	dec	$W_{mx}$	$e_{Wm50}$	$z_{hel}$	$z_{cmb}$	Flux	$w_1$	$e_{w1}$	$i$	$\mu$
J100321-291708		150.838	-29.286	96	16	0.0517491	0.0529012	0.84	16.974	0.139	44	34.06
J100342-270137	29166	150.925	-27.027	182	16	0.0031855	0.0043016	47.59	13.592	0.027	87	31.68
J100351-273417	29179	150.963	-27.571	328	16	0.0093131	0.0104323	15.74	11.331	0.023	54	32.75
J100426-282638	29216	151.108	-28.444	194	14	0.0036125	0.0047197	34.31	12.884	0.024	70	31.49
J100634-295615	29366	151.642	-29.938	140	17	0.0037259	0.0048245	9.71	11.106	0.021	63	28.59
J100640-273917	29378	151.667	-27.655	199	18	0.0142332	0.015361	2.26	14.574	0.035	63	33.54
J100700-273944		151.750	-27.662	111	18	0.0141531	0.0152813	1.21	14.231	0.036	53	31.26
J100713-262336	768336	151.804	-26.393	125	16	0.015354	0.0164928	2.23	15.138	0.04	67	32.05
J100746-281451	3751428	151.942	-28.247	151	19	0.0156942	0.0168207	0.45	11.891	0.026	40	31.1
J100808-260942	29470	152.033	-26.162	112	15	0.0102838	0.0114197	1.95	15.422	0.046	67	31.88
J100830-262140	768685	152.125	-26.361	115	18	0.013983	0.0151222	0.91	15.732	0.053	80	32.02
J100903-290239	29530	152.262	-29.044	247	14	0.0036825	0.0047913	143.29	16.596	0.091	55	36.78
J100938-255850	29553	152.408	-25.981	139	17	0.0102905	0.0114296	4.31	12.944	0.025	69	30.23
J100939-290112	154738	152.412	-29.020	207	16	0.0468858	0.0480433	1.22	13.136	0.026	51	32.9
J101006-265322	762605	152.525	-26.889	109	18	0.0282395	0.0293931	0.96	16.117	0.073	62	32.66
J101018-285748	29602	152.575	-28.963	136	17	0.0138496	0.0149718	1.0	14.777	0.036	49	32.85
J101025-275214	748738	152.604	-27.871	124	15	0.0080756	0.0091999	1.46	15.021	0.041	68	31.87
J101049-302538	29641	152.704	-30.427	182	17	0.0090463	0.0101521	4.11	14.316	0.03	71	32.65
J101236-272905	754250	153.150	-27.485	187	18	0.0319654	0.033122	0.83	15.01	0.038	44	34.78
J101247-275028	29743	153.196	-27.841	340	15	0.0087194	0.0098475	14.46	10.558	0.022	53	32.18
J101247-291053	732369	153.196	-29.181	236	19	0.030828	0.0319704	0.82	14.172	0.031	69	33.68
J101314-271308	3752634	153.308	-27.219	188	18	0.0151772	0.0163176	1.15	12.844	0.026	39	33.07
J101348-273147	29821	153.450	-27.530	139	16	0.008686	0.0098176	1.5	15.431	0.046	68	32.73
J101359-253824	29836	153.496	-25.640	194	15	0.0106274	0.0117746	5.47	14.827	0.045	61	33.77
J101441-285221	29892	153.671	-28.872	297	18	0.0036792	0.0047961	11.79	9.651	0.023	83	29.78
J101443-263328	766603	153.679	-26.558	255	19	0.0536138	0.0548041	1.39	16.823	0.12	52	37.4
J101448-274240	750927	153.700	-27.711	155	18	0.0141098	0.0152473	1.9	15.221	0.044	56	33.45
J101448-285723	29903	153.700	-28.956	383	16	0.0139663	0.0150942	1.92	11.286	0.023	70	32.71
J101526-264259	764730	153.858	-26.716	222	16	0.0329628	0.0341296	0.6	14.08	0.029	47	34.36
J101531-292423	29945	153.879	-29.406	309	15	0.0305878	0.0317313	1.75	13.269	0.026	74	33.76
J101613-291212	29987	154.054	-29.203	413	19	0.0364119	0.0375643	2.02	11.979	0.023	46	34.87
J101618-301143		154.075	-30.195	177	18	0.0366987	0.0378433	1.11	14.598	0.038	46	34.02
J101632-291258		154.133	-29.216	171	17	0.0140164	0.0151442	1.57	15.258	0.046	65	33.55
J101725-285259	3081722	154.354	-28.883	161	13	0.0413119	0.0424738	0.72	13.459	0.027	56	31.9
J101756-285557		154.483	-28.933	158	17	0.0365386	0.0376953	0.87	15.135	0.042	63	33.21
J101826-264356	3753777	154.608	-26.732	140	15	0.030908	0.0320758	0.92	13.685	0.032	43	32.34
J101843-281718	743506	154.679	-28.288	237	19	0.0411918	0.0423598	1.33	12.274	0.024	39	33.44
J101927-264159	764945	154.863	-26.700	85	16	0.0080509	0.0096496	0.77	16.06	0.067	62	31.57
J101945-272719	30186	154.938	-27.455	264	18	0.0364752	0.0376454	0.79	13.967	0.056	45	35.08
J102017-253913	30216	155.071	-25.654	118	16	0.0114913	0.0126466	4.52	14.939	0.04	52	32.27
J102019-285220	30218	155.079	-28.872	418	18	0.0312183	0.0323721	1.14	11.54	0.024	75	33.26
J102030-260951	30324	155.125	-26.164	313	18	0.0560488	0.0572516	2.14	13.826	0.028	58	34.98
J102048-292635	729284	155.200	-29.443	145	18	0.0300074	0.0311558	0.83	15.655	0.052	48	34.13
J102053-265610	30257	155.221	-26.936	526	18	0.0332764	0.0344448	3.04	11.509	0.024	73	34.21
J102054-263844	765548	155.225	-26.646	117	18	0.0412118	0.0423947	0.74	15.548	0.051	43	33.52
J102059-265129	763013	155.246	-26.858	171	17	0.0385051	0.0350231	0.48	14.736	0.052	54	33.53
J102100-273339	753130	155.250	-27.561	210	16	0.0332597	0.0344268	0.66	14.955	0.039	64	34.15
J102110-261638	3754419	155.292	-26.277	244	18	0.0557719	0.0569743	1.55	13.081	0.025	67	32.85
J102111-274340	3754421	155.296	-27.728	155	17	0.0562389	0.0574309	0.77	13.604	0.048	54	32.03
J102115-250342	783072	155.312	-25.062	249	15	0.0327493	0.033934	1.06	14.514	0.034	57	34.69
J102155-260232		155.479	-26.042	123	18	0.0370189	0.0382024	0.96	14.522	0.035	54	31.97
J102233-294017	726509	155.637	-29.671	148	17	0.0260447	0.0271886	1.6	16.504	0.091	59	34.43
J102328-253424	777390	155.867	-25.573	372	16	0.0405058	0.0417004	1.64	12.876	0.025	53	34.95
J102336-264751	3754999	155.900	-26.797	121	18	0.0352344	0.0364122	0.88	15.63	0.056	48	33.38
J102338-264531	764220	155.908	-26.759	235	16	0.0346406	0.0358181	0.89	14.603	0.032	72	34.03
J102411-285533	30492	156.046	-28.926	169	18	0.0129556	0.0140925	1.65	13.838	0.03	45	33.08
J102413-284853	737129	156.054	-28.815	164	19	0.0373692	0.0385344	1.05	17.006	0.149	45	36.23
J102416-270241	760541	156.067	-27.045	193	18	0.0346139	0.0357899	0.73	14.973	0.039	46	34.73
J102416-284343	3167291	156.067	-28.729	167	19	0.0263949	0.0275486	0.51	10.887	0.021	60	29.29
J102430-290904	732726	156.125	-29.151	117	18	0.0124986	0.0136336	0.81	15.043	0.041	63	31.8
J102439-274841	749549	156.162	-27.811	104	17	0.0120116	0.0131566	1.09	16.106	0.072	49	33.09
J102600-280334		156.500	-28.059	142	17	0.0363918	0.0375637	0.76	16.358	0.082	68	33.82
J102601-255556	773492	156.504	-25.932	244	18	0.0399843	0.0411762	3.15	12.993	0.025	39	34.32
J102621-291150	732211	156.588	-29.197	86	17	0.0123152	0.0134513	1.68	15.441	0.049	45	31.95
J102636-245116	30681	156.650	-24.854	126	18	0.0132759	0.0144449	1.05	15.145	0.042	46	33.16
J102637-264142	764986	156.654	-26.695	95	17	0.0313684	0.0325455	0.5	15.797	0.056	56	32.08
J102643-261256	770222	156.679	-26.216	271	19	0.033213	0.0343958	1.22	13.218	0.025	47	34.31
J102719-253256	30748	156.829	-25.549	211	16	0.0115713	0.0127345	1.48	2.628	0.011	74	21.52
J102738-294752	30772	156.908	-29.798	144	14	0.0128255	0.0139584	2.96	14.994	0.038	61	32.72
J102844-265319	762625	157.183	-26.889	143	19	0.036075	0.037258	2.12	12.858	0.024	54	30.92
J102931-281028	744919	157.379	-28.174	119	18	0.0600515	0.0612526	1.15	12.892	0.024	48	30.59
J102934-261937	30912	157.392	-26.327	160	17	0.0131091	0.0142706	1.07	13.618	0.026	83	31.23
J103002-284116	738653	157.508	-28.688	109	18	0.0127989	0.0139428	0.85	15.035	0.04	67	31.39
J103015-270743	759425	157.562	-27.129	201	17	0.0363085	0.0374913	0.79	14.969	0.037	46	34.93
J103114-295837	722930	157.808	-29.977	94	15	0.0139797	0.0151154	0.8	15.799	0.05		

J103130-251020	781903	157.875	-25.172	106	19	0.0356613	0.0368586	0.91	14.423	0.033	42	32.02
J103240-282058	742765	158.167	-28.349	172	18	0.013079	0.0142281	1.43	13.946	0.029	83	31.86
J103241-273137	31149	158.171	-27.527	140	19	0.0127555	0.0139105	0.57	13.62	0.028	76	30.77
J103244-283639	31154	158.183	-28.611	541	17	0.0120617	0.0132076	3.61	9.926	0.023	80	32.58
J103248-273119	31161	158.200	-27.522	192	17	0.0120383	0.0131927	1.73	13.051	0.027	39	33.35
J103250-301601	31162	158.208	-30.267	133	18	0.0115914	0.0127233	3.7	13.944	0.03	49	31.95
J103257-250937	782023	158.238	-25.160	215	18	0.0244736	0.0256592	1.05	15.624	0.051	79	34.52
J103258-274013	31171	158.242	-27.670	120	16	0.0104572	0.0116088	1.73	15.271	0.044	66	32.05
J103322-271142	758476	158.342	-27.195	188	19	0.0359749	0.0371595	1.27	13.694	0.028	50	33.08
J103335-272717	31217	158.396	-27.455	547	18	0.0113245	0.0124792	3.97	9.758	0.024	68	32.7
J103353-274945	31238	158.471	-27.829	187	19	0.009173	0.0103226	1.81	14.656	0.037	60	33.48
J103359-272013	31243	158.496	-27.337	114	15	0.0325825	0.0337627	2.05	11.984	0.023	61	28.77
J103359-301003	31242	158.496	-30.168	400	19	0.0116414	0.0127751	3.29	10.959	0.021	83	32.33
J103420-265408	92288	158.583	-26.902	133	19	0.012462	0.0136226	1.26	15.119	0.04	90	31.93
J103436-273900	31293	158.650	-27.650	242	17	0.0100936	0.0112462	3.44	13.415	0.217	47	33.97
J103507-275923	31334	158.779	-27.990	162	18	0.0081156	0.0092637	1.11	12.882	0.026	63	31.0
J103521-272324	755655	158.838	-27.390	92	17	0.0104839	0.0116395	0.68	15.357	0.049	39	32.62
J103523-281855	31360	158.846	-28.315	320	17	0.0110043	0.0121534	6.45	11.382	0.023	44	33.32
J103541-265827	761496	158.921	-26.974	95	17	0.0086727	0.0098294	0.73	15.53	0.05	61	31.54
J103546-273840	751896	158.942	-27.644	89	17	0.0158543	0.0170144	1.19	16.421	0.099	44	33.16
J103547-290131	31390	158.946	-29.025	240	18	0.0326426	0.0338108	1.87	17.097	0.161	55	37.22
J103602-261141	770447	159.008	-26.195	107	17	0.0109376	0.0121028	0.64	15.561	0.05	50	32.62
J103602-272938	754118	159.008	-27.494	145	18	0.0388836	0.0400713	0.51	16.391	0.091	46	35.04
J103603-245430	784823	159.012	-24.908	139	16	0.0131358	0.0143123	1.7	16.089	0.081	76	33.22
J103621-252235	31440	159.088	-25.376	115	19	0.0133826	0.0145566	1.58	12.411	0.024	44	30.2
J103644-251543	31482	159.183	-25.262	132	18	0.0122418	0.0134155	1.21	14.767	0.033	63	32.06
J103645-281010	744989	159.188	-28.169	123	17	0.0116314	0.0127833	1.98	15.134	0.051	56	32.43
J103646-293253	31484	159.192	-29.548	154	14	0.0119049	0.0130461	2.11	16.794	0.134	66	34.46
J103650-270902	31490	159.208	-27.151	271	18	0.0374059	0.0385951	1.9	13.641	0.028	39	35.43
J103651-260227	31491	159.213	-26.041	156	16	0.0079088	0.0090722	3.67	17.025	0.148	65	34.91
J103653-270311	31494	159.221	-27.053	191	17	0.0118382	0.0129899	2.57	13.646	0.029	46	33.32
J103701-284018	738882	159.254	-28.672	215	16	0.0325158	0.0336877	0.87	14.885	0.037	73	33.91
J103704-252038	31514	159.267	-25.344	194	17	0.0123652	0.0135388	1.7	13.543	0.027	84	31.94
J103712-274108	3167313	159.300	-27.686	168	19	0.0094365	0.01059	1.65	16.431	0.092	62	34.74
J103722-273235	753342	159.342	-27.543	98	19	0.0091964	0.0103507	0.69	15.388	0.053	49	32.14
J103726-261843	31557	159.358	-26.312	186	18	0.0117248	0.0128911	2.01	14.563	0.035	43	34.34
J103749-270715	759579	159.454	-27.121	137	18	0.0081523	0.009309	1.76	12.296	0.024	39	31.21
J103803-281007	31602	159.512	-28.169	291	17	0.035161	0.0363407	1.78	14.483	0.032	75	34.73
J103809-260453	31612	159.537	-26.081	138	19	0.0119082	0.0130769	0.53	14.679	0.041	70	31.92
J103818-285307	31626	159.575	-28.885	287	17	0.0146335	0.0157842	5.52	17.263	0.189	72	37.45
J103821-254126	776142	159.588	-25.691	83	16	0.0114446	0.0126156	1.0	15.021	0.045	39	31.82
J103833-274357	31638	159.637	-27.733	141	16	0.0147135	0.0158736	2.92	16.958	0.144	42	35.72
J103840-283405	31642	159.667	-28.568	292	18	0.0115747	0.0127247	1.39	11.269	0.026	46	32.73
J103841-253530	31644	159.671	-25.592	142	16	0.0128122	0.0139857	1.58	14.764	0.036	50	32.98
J103842-281535	6728765	159.675	-28.260	133	17	0.0113579	0.0125101	0.79	17.402	0.195	82	34.26
J103902-291255	31664	159.758	-29.215	147	18	0.0106707	0.0118148	1.44	15.609	0.054	52	33.86
J103915-301757	31677	159.812	-30.299	419	17	0.012532	0.0136693	11.38	10.289	0.022	85	31.84
J103918-265030	31683	159.825	-26.842	328	16	0.0102671	0.0114292	3.2	11.654	0.023	71	32.42
J103922-293505	31690	159.842	-29.585	207	16	0.0129456	0.0140895	3.82	15.208	0.049	67	34.21
J103926-265812	31694	159.858	-26.970	187	18	0.0354212	0.0366114	1.06	11.638	0.024	40	31.75
J103939-280552	745884	159.912	-28.098	127	18	0.0113445	0.0124987	1.16	15.431	0.051	64	32.51
J104000-292445	31732	160.000	-29.413	169	17	0.0125654	0.0137106	3.02	16.068	0.074	63	34.38
J104004-301606	31738	160.017	-30.268	261	16	0.0113479	0.0124846	4.75	11.978	0.026	70	31.83
J104016-274630	31754	160.067	-27.775	310	15	0.0132592	0.0144184	12.21	12.674	0.028	56	33.78
J104048-281302	31792	160.200	-28.217	158	16	0.0354812	0.0366627	1.1	13.986	0.044	71	31.81
J104058-274546	750199	160.242	-27.763	150	17	0.0133059	0.0144657	1.34	15.609	0.053	64	33.39
J104059-270456	31805	160.246	-27.082	330	15	0.0158209	0.0169888	6.42	11.934	0.024	65	32.92
J104100-284430	31809	160.250	-28.742	159	17	0.0125053	0.0136566	1.57	13.495	0.026	62	31.57
J104139-254049	160.412	-25.680	100	15	0.0128689	0.0140438	1.05	15.713	0.055	44	32.9	
J104139-274633	31852	160.412	-27.777	118	19	0.0145367	0.0156983	1.03	16.608	0.105	65	33.37
J104157-264302	160.488	-26.717	229	19	0.0366687	0.0378639	0.96	14.61	0.045	59	34.36	
J104221-291748	31901	160.588	-29.297	98	18	0.0147569	0.015907	1.72	16.455	0.092	58	32.7
J104245-264738	31924	160.688	-26.794	292	16	0.0355446	0.0367384	1.74	15.619	0.051	39	37.7
J104252-252014	160.717	-25.337	95	18	0.0212714	0.0224592	0.66	14.122	0.03	60	30.18	
J104309-300301	31948	160.787	-30.050	134	17	0.0106774	0.0118171	6.86	13.885	0.028	51	31.81
J104311-261500	31951	160.796	-26.250	377	15	0.0151171	0.0162916	6.41	11.081	0.022	64	32.64
J104326-251857	31960	160.858	-25.316	94	18	0.012552	0.0137302	1.04	16.81	0.12	44	33.71
J104339-285157	31981	160.912	-28.866	276	15	0.0115647	0.0127155	4.61	11.602	0.02	73	31.62
J104414-271548	757564	161.058	-27.263	194	18	0.0366053	0.0377977	0.41	15.102	0.042	42	35.24
J104422-290119	734399	161.175	-29.022	118	17	0.0335999	0.0347751	0.94	14.122	0.028	58	31.21
J104447-270553	759885	161.196	-27.098	163	17	0.0362484	0.0374419	0.8	15.689	0.055	72	33.61
J104603-291551	3760243	161.512	-29.264	98	17	0.0308046	0.0319753	0.84	17.328	0.187	51	34.02
J104620-293733	727073	161.583	-29.626	226	18	0.0394339	0.0406115	1.29	14.223	0.03	58	33.97
J104629-253308	32175	161.621	-25.552	133	18	0.012005	0.0131826	1.35	15.66	0.053	60	33.07
J104637-263911	3760383	161.654	-26.653	325	19	0.0388269	0.0400277	0.76	14.427	0.077	45	36.42
J104905-292232	32361	162.271	-29.376	107	17	0.0142499	0.0154023	4.07	13.668	0.029	58	30.27

Table 3:: Norma HI data from WALLABY phase 1 pilot survey.

name	PGC	ra	dec	$W_{mx}$	$e_{Wm50}$	$z_{hel}$	$z_{cmb}$	Flux	$w_1$	$e_{w1}$	$i$	$\mu$
J163435-620248	58527	248.646	-62.047	209	17	0.0148836	0.0151111	4.84	13.359	0.024	66	32.41
J163452-603705	58536	248.717	-60.618	176	17	0.0109075	0.0111358	15.21	9.709	0.023	69	27.96
J163455-610147	3078514	248.729	-61.030	139	18	0.0175488	0.0177778	2.66	14.094	0.033	40	32.97
J163512-580438	58547	248.800	-58.077	272	15	0.0091663	0.0093973	12.63	7.105	0.027	44	28.38
J163518-581311	58549	248.825	-58.220	218	16	0.0052069	0.0054365	11.9	10.736	0.026	68	29.89
J163834-601517		249.642	-60.255	151	19	0.0114879	0.0117072	1.69	8.511	0.023	44	27.39
J163927-594844	3078607	249.863	-59.812	435	19	0.037636	0.0378591	1.52	13.914	0.034	53	36.62
J164107-605902	58755	250.279	-60.984	158	15	0.0116547	0.0118664	3.36	14.968	0.037	83	32.53
J164113-603202		250.304	-60.534	156	19	0.0396508	0.0398685	1.2	14.946	0.037	77	32.6
J164146-580424	3078655	250.442	-58.073	251	19	0.0472927	0.0475132	1.35	12.408	0.025	63	32.39
J164249-610527	92488	250.704	-61.091	306	17	0.0148569	0.0150647	3.95	11.813	0.024	59	32.72
J164355-620233	349886	250.979	-62.042	303	19	0.0391237	0.0393325	1.37	13.106	0.025	52	34.38
J164455-575030	3078727	251.229	-57.842	294	18	0.0408056	0.0482681	1.25	13.037	0.027	58	33.92
J164508-611614		251.283	-61.271	169	15	0.0122652	0.0124662	2.55	14.619	0.039	56	33.22
J164523-580908	3078738	251.346	-58.152	300	19	0.0474528	0.0476627	1.16	13.902	0.033	55	34.97
J164619-614832		251.579	-61.809	150	18	0.0104706	0.0106678	1.34	13.677	0.028	46	32.38
J164644-601351	365061	251.683	-60.231	297	18	0.053	0.0532056	1.06	13.309	0.027	51	34.58
J164727-575143	3078771	251.863	-57.862	322	18	0.0475062	0.0477101	1.01	12.89	0.033	40	35.31
J164749-613936		251.954	-61.660	156	17	0.0175088	0.0177036	3.37	15.824	0.089	45	34.74
J164826-623040	343635	252.108	-62.511	165	19	0.0147702	0.0149624	2.34	13.793	0.031	58	32.19
J164934-600157		252.392	-60.032	109	19	0.0157275	0.0159184	1.03	12.764	0.026	45	30.27
J164950-623318	4077412	252.458	-62.555	92	17	0.0142932	0.0144818	2.85	15.942	0.074	49	32.42
J165101-604809	59111	252.754	-60.803	442	19	0.0109276	0.0111133	6.16	12.878	0.027	50	35.73
J165131-603514	59130	252.879	-60.587	121	17	0.0111444	0.0113289	1.68	14.854	0.046	48	32.53
J165140-601629	4585661	252.917	-60.275	119	18	0.0471526	0.0473434	0.77	15.946	0.066	52	33.39
J165152-592813	3078870	252.967	-59.470	290	19	0.04815	0.0483406	0.94	14.236	0.042	65	34.76
J165223-591245		253.096	-59.212	130	19	0.0470392	0.0472283	0.78	15.918	0.111	42	34.4
J165247-584019	165944	253.196	-58.672	151	18	0.0084092	0.0085902	1.23	12.008	0.023	38	31.35
J165248-585644	59180	253.200	-58.946	281	18	0.0096433	0.0098245	1.15	12.574	0.074	71	32.7
J165248-591309	59175	253.200	-59.219	292	14	0.0049501	0.0051304	63.36	8.798	0.021	56	29.64
J165249-574157		253.204	-57.699	101	17	0.0097	0.0098813	0.93	14.961	0.057	60	31.27
J165331-595759	3080099	253.379	-59.966	147	15	0.0155741	0.0157543	1.85	15.576	0.055	39	34.8
J165439-605730		253.662	-60.958	158	15	0.0103672	0.0105433	1.7	15.252	0.046	76	32.91
J165520-592615	3078940	253.833	-59.438	148	19	0.016378	0.0165533	1.5	14.086	0.032	49	32.56
J165559-592439	165948	253.996	-59.411	196	18	0.0159811	0.0161545	2.46	12.224	0.024	39	32.61
J165632-594959	4584387	254.133	-59.833	382	18	0.0478431	0.0480205	1.08	12.57	0.031	57	34.54
J165644-622413	4075676	254.183	-62.404	340	17	0.0170218	0.0171936	6.62	11.642	0.023	62	32.88
J165647-614814	352206	254.196	-61.804	259	19	0.0292869	0.0294607	1.33	6.651	0.038	76	26.38
J165758-624336	59334	254.492	-62.727	359	19	0.0167182	0.016887	6.07	10.758	0.024	67	32.01
J165840-582909	141869	254.667	-58.486	251	18	0.0204708	0.0206373	1.43	12.548	0.027	57	32.74
J165949-584125	59399	254.954	-58.690	180	15	0.0158843	0.0160469	8.73	12.414	0.025	55	31.32
J170034-622407	345097	255.142	-62.402	415	19	0.0481133	0.0482805	1.9	12.926	0.025	63	34.99
J170116-621215	165971	255.317	-62.204	333	18	0.0462086	0.0463736	1.44	12.572	0.024	42	34.97
J170149-603901	165952	255.454	-60.650	264	19	0.016338	0.0164961	1.56	12.958	0.026	39	34.52
J170232-584322	165953	255.633	-58.723	273	18	0.0204875	0.0206432	1.33	12.148	0.025	41	33.75
J170303-614604	59497	255.762	-61.768	163	14	0.009083	0.0092374	16.56	13.377	0.029	44	32.53
J170550-620939	348516	256.458	-62.161	157	16	0.0050368	0.0051839	1.16	15.434	0.052	43	34.5
J170642-604341	360946	256.675	-60.728	117	19	0.0267585	0.0269052	1.08	15.094	0.046	47	32.76
J170659-620502	59635	256.746	-62.084	223	13	0.0050335	0.0051776	56.53	11.735	0.022	86	30.67
J170747-595059	59659	256.946	-59.850	276	16	0.0156542	0.0157955	5.78	13.111	0.037	76	33.07
J170915-613637	165957	257.312	-61.610	257	17	0.0140897	0.0142289	6.43	11.746	0.023	53	32.21
J170937-602429		257.404	-60.408	109	17	0.0157642	0.0159013	1.3	15.431	0.053	58	32.16
J171015-615505	59737	257.562	-61.918	252	15	0.0160945	0.0162316	6.74	11.926	0.022	47	32.71
J171309-603124	362690	258.288	-60.523	118	19	0.0160878	0.0162156	1.29	14.766	0.041	65	31.52
J171338-590621	59880	258.408	-59.106	134	14	0.0117381	0.0118619	12.08	12.676	0.026	54	30.41
J171339-615822	92494	258.413	-61.973	137	16	0.0149237	0.0150521	1.35	14.554	0.035	75	31.64
J171500-601723		258.750	-60.290	206	18	0.0197136	0.0198365	1.24	15.327	0.051	53	34.93
J171538-602409		258.908	-60.403	240	19	0.0193934	0.0195147	1.62	14.233	0.031	60	34.12
J171804-575135	60032	259.517	-57.860	149	13	0.0036092	0.0037173	54.11	13.244	0.027	80	30.57
J171850-601104	365445	259.708	-60.184	186	16	0.0154007	0.0155125	1.72	14.833	0.041	48	34.32
J171924-615016	92496	259.850	-61.838	267	17	0.0244436	0.0245582	2.49	14.359	0.051	70	34.33
J172007-600928	60092	260.029	-60.158	335	18	0.0150337	0.015142	9.39	11.359	0.023	57	32.73

Table 4:: Eridanus HI data from WALLABY phase 1 pilot survey.

name	PGC	ra	dec	$W_{mx}$	$e_{Wm50}$	$z_{hel}$	$z_{cmb}$	Flux	$w_1$	$e_{w1}$	$i$	$\mu$
J034114-235017	13561	55.308	-23.838	199	19	0.006281	0.0059107	3.22	13.513	0.236	73	32.17
J033859-223502	13442	54.746	-22.584	152	16	0.0144767	0.0140858	3.0	15.313	0.044	67	33.03
J033854-2262013	13434	54.725	-26.337	463	15	0.0046365	0.0042711	30.74	12.869	0.03	85	34.82
J034056-223350	13544	55.233	-22.564	339	18	0.0051669	0.0047884	8.38	9.131	0.023	60	30.39
J034517-230001	13760	56.321	-23.000	300	18	0.0051869	0.0048308	2.44	11.209	0.025	75	31.51
J034219-224520	13608	55.579	-22.756	114	17	0.0052269	0.0048558	2.44	15.569	0.049	48	32.98
J034057-214245	13543	55.237	-21.712	143	15	0.0056606	0.0052773	2.44	13.072	0.026	76	30.31

J034040-221711	13531	55.167	-22.286	151	16	0.0059141	0.0055325	1.91	14.519	0.033	79	31.94
J034858-220751	13894	57.242	-22.131	214	18	0.0140797	0.0137329	1.49	10.447	0.022	49	30.44
J034814-212824	13871	57.058	-21.473	225	17	0.005287	0.0049363	1.88	12.942	0.027	48	33.16
J034337-211418	13689	55.904	-21.238	123	15	0.005367	0.0049936	2.84	14.831	0.037	67	31.67
J034131-214051	13569	55.379	-21.681	152	16	0.0054504	0.0050696	2.08	12.134	0.025	62	30.02
J033921-212450	13460	54.837	-21.414	108	16	0.0054238	0.0050315	1.03	13.753	0.03	55	30.55
J033537-211742	13283	53.904	-21.295	142	15	0.0060308	0.0056206	5.97	14.758	0.038	81	31.89
J033341-212844	13184	53.421	-21.479	199	15	0.0062076	0.0057895	9.03	11.882	0.024	63	30.84
J033351-212725	13194	53.462	-21.457	168	16	0.0135661	0.0131455	5.84	14.648	0.289	44	33.95
J033810-194412	13401	54.542	-19.737	167	19	0.0139363	0.013526	2.59	15.639	0.056	60	34.02
J033757-213938	13392	54.487	-21.661	131	19	0.0138763	0.0134756	1.11	14.676	0.052	42	33.12
J032434-215824	12746	51.142	-21.973	142	18	0.0145401	0.01408	1.37	14.492	0.029	45	33.06
J032425-213233	12737	51.104	-21.543	326	15	0.0053003	0.0048412	23.1	11.296	0.023	81	31.84
J033327-213352	13172	53.362	-21.564	118	18	0.0050068	0.0045886	0.99	10.51	0.022	49	27.98
J033527-211302	831168	53.862	-21.217	90	15	0.0050735	0.0046624	1.97	14.956	0.038	58	30.87
J032735-211339	12889	51.896	-21.227	161	17	0.0056239	0.0051769	3.09	14.003	0.029	84	31.62
J033653-245445	13342	54.221	-24.913	106	18	0.0061342	0.0057507	2.49	13.884	0.031	66	30.14
J033302-240756	13154	53.258	-24.132	154	17	0.0063878	0.0059822	6.37	14.998	0.039	82	32.45
J033501-245556	13255	53.754	-24.932	388	16	0.0048767	0.0044855	55.96	9.638	0.023	55	31.71
J033728-243010	13368	54.367	-24.503	180	16	0.0050001	0.0046172	21.32	10.353	0.02	42	30.1
J033617-253615	13304	54.071	-25.604	115	18	0.0053137	0.004932	1.65	13.324	0.027	52	30.51
J033326-234246	13171	53.358	-23.713	249	17	0.0060542	0.005648	5.11	11.516	0.023	61	31.48
J033351-210313	13198	53.462	-21.054	149	18	0.0224355	0.022009	2.57	13.125	0.026	58	31.13

Table 5:: NGC4636 HI data from WALLABY phase 1 pilot survey.

name	PGC	ra	dec	$W_{mx}$	$e_{Wm50}$	$z_{hel}$	$z_{cmb}$	Flux	$w_1$	$e_{w1}$	$i$	$\mu$
J122708+055255	40801	186.783	5.882	164	18	0.0037126	0.0048539	13.46	13.103	0.025	72	31.0
J122726+061551	40851	186.858	6.264	131	15	0.00483	0.0059703	6.07	13.085	0.185	49	31.0
J122733+061359	40875	186.887	6.233	136	17	0.0213648	0.0225237	3.78	13.484	0.026	40	32.26
J122755+054312	40933	186.979	5.720	135	16	0.0074985	0.0086435	0.7	12.654	0.026	80	29.59
J122852+041739	41088	187.217	4.294	286	15	0.0141298	0.015287	9.39	12.571	0.026	0	
J122930+074142	41170	187.375	7.695	176	18	0.0025084	0.0036351	2.04	12.74	0.026	57	31.42
J122932+005020	41177	187.383	.839	117	17	0.0074618	0.0086225	1.64	15.867	0.065	46	33.51
J123022+034431	41307	187.592	3.742	310	17	0.0141031	0.0152598	5.65	15.146	0.048	43	37.05
J123026+041450	41317	187.608	4.247	310	17	0.0141031	0.0152576	5.65	11.382	0.023	62	32.22
J123138+035620	41471	187.908	3.939	146	13	0.005774	0.0069181	45.94	14.379	0.034	61	32.13
J123156+035316	97234	187.983	3.888	143	15	0.0149804	0.0161346	1.9	14.892	0.045	45	33.52
J123209-010543	1126897	188.037	-1.095	121	16	0.0080155	0.0091771	1.33	15.721	0.059	69	32.44
J123228+002315	4105156	188.117	.388	146	15	0.0050935	0.0062474	41.21	14.712	0.037	80	31.97
J123236+023943	41599	188.150	2.662	137	16	0.005784	0.0069312	11.09	14.283	0.031	51	32.3
J123244+000656	41618	188.183	.116	301	13	0.0037493	0.0049018	132.95	10.693	0.023	0	
J123249+031748	41625	188.204	3.297	191	16	0.0166382	0.0177949	2.88	13.912	0.029	43	33.84
J123422+021914	41816	188.592	2.321	114	16	0.0058907	0.0070359	2.63	12.633	0.027	68	29.12
J123424+062511	4332429	188.600	6.420	153	15	0.0067347	0.0078636	56.62	16.022	0.076	40	35.26
J123427+021108	41823	188.613	2.186	313	16	0.0060142	0.0071598	65.45	8.518	0.022	53	29.82
J123510-001308	41911	188.792	-.219	482	18	0.0230093	0.0241801	3.88	11.019	0.023	56	33.95
J123530-021940	41941	188.875	-2.328	453	17	0.0239099	0.0250585	5.09	11.071	0.023	59	33.61
J123554-015112	41998	188.975	-1.853	216	15	0.0229525	0.0241257	4.05	14.105	0.032	57	33.68
J123609+073152	1324268	189.037	7.531	272	18	0.0240166	0.0251558	1.07	12.274	0.032	47	33.38
J123630+001315	1160233	189.125	.221	136	13	0.0123986	0.0135535	4.41	15.081	0.044	63	32.48
J123641+030621	42080	189.171	3.106	120	16	0.0048033	0.0059399	7.31	15.602	0.059	69	32.27
J123734+042150	42152	189.392	4.364	171	16	0.0176656	0.01881	2.21	12.924	0.028	79	30.87
J123802+001036	1159012	189.508	.177	102	17	0.0134226	0.0145758	1.22	15.822	0.068	41	33.3
J123805-000137	42202	189.521	-.027	311	13	0.0125053	0.0136579	5.23	11.403	0.023	64	32.16
J123805-002419	1144183	189.521	-.405	179	16	0.0254409	0.0266092	0.52	15.681	0.058	43	35.36
J123827+041912	42241	189.613	4.320	242	19	0.0026352	0.0037611	1.49	10.024	0.022	59	29.93
J123835+012413	42255	189.646	1.404	284	16	0.0173353	0.0184882	4.68	13.097	0.029	58	33.75
J123905-020044	1103962	189.771	-.2012	100	17	0.0087761	0.0099269	1.09	15.535	0.055	54	32.05
J123911+004305	42317	189.796	.718	212	13	0.0169817	0.0181351	6.8	13.242	0.029	39	33.94
J123912+060038	42319	189.800	6.011	289	19	0.0080889	0.009212	3.21	11.172	0.024	57	31.92
J123928+041549	42354	189.867	4.264	261	18	0.040906	0.0502669	0.7	12.772	0.026	57	33.21
J123948-014620	1110510	189.950	-1.772	115	17	0.0141898	0.0153449	1.47	15.437	0.052	52	32.66
J123949+014016	42393	189.954	1.671	95	16	0.0040795	0.005214	2.0	14.538	0.035	84	29.99
J123955-000822	1150986	189.979	-.139	125	15	0.0102237	0.0113703	2.96	16.286	0.1	52	33.85
J124002-033623	42409	190.008	-3.606	99	18	0.0084759	0.0096271	5.5	15.262	0.05	58	31.56
J124109+041725	1266160	190.287	4.290	97	18	0.0288433	0.0299932	0.64	14.96	0.04	62	31.03
J124111-013526	42538	190.296	-1.591	180	15	0.0133292	0.0144801	3.21	14.414	0.034	53	33.42
J124111+012435	42542	190.296	1.410	166	13	0.0056706	0.006805	5.97	11.793	0.024	56	30.3
J124121+001315	1160198	190.338	.221	128	17	0.0159977	0.0171469	0.86	16.205	0.087	66	33.26
J124123-030327	42559	190.346	-3.058	90	16	0.0048333	0.0059769	2.72	12.926	0.026	55	28.95
J124128-031517	91219	190.367	-3.255	106	17	0.0059975	0.0071425	0.76	15.694	0.058	84	31.59
J124231+035729	42688	190.629	3.958	126	17	0.002475	0.003594	6.08	11.313	0.024	53	28.82
J124232-000459	42689	190.633	-.083	216	16	0.0057406	0.0068766	45.29	10.967	0.023	68	30.1
J124232-012111	42692	190.633	-1.353	140	15	0.0037059	0.0048426	25.15	13.775	0.03	47	32.14
J124237-020708	3106365	190.654	-2.119	199	17	0.0459618	0.0471478	0.3	14.555	0.034	45	34.56

J124240+012047	42709	190.667	1.346	262	16	0.0167416	0.0178855	4.57	13.045	0.028	50	33.78
J124247+012239	1193027	190.696	1.377	149	19	0.0330195	0.0341814	0.53	15.135	0.043	54	33.35
J124257-011345	42747	190.738	-1.229	307	15	0.0107041	0.0118475	17.04	12.456	0.026	67	33.06
J124317-003841	42791	190.821	-.645	289	14	0.0088228	0.009962	6.65	11.842	0.027	69	32.14
J124333+014827	92947	190.887	1.808	153	18	0.0484302	0.0496063	0.73	12.675	0.024	71	30.4
J124350-003344	42847	190.958	-.562	199	15	0.0087694	0.0099072	21.88	12.185	0.025	65	31.06
J124421+042536	42892	191.088	4.427	265	19	0.0285798	0.029722	2.09	12.602	0.023	54	33.22
J124428-030017	42909	191.117	-3.005	346	17	0.0238765	0.0250351	3.49	11.881	0.023	62	33.18
J124433-021916	42921	191.137	-2.321	110	15	0.0053037	0.0064398	13.2	15.052	0.042	49	32.28
J124506+053842	1286794	191.275	5.645	157	17	0.021258	0.0223851	2.0	14.131	0.03	63	32.16
J124508-002747	42975	191.283	-.463	386	14	0.0050635	0.0061942	85.89	8.342	0.021	82	29.57
J124531-003203	3110155	191.379	-.534	134	15	0.0053971	0.0065275	13.51	13.092	0.026	43	31.56
J124608+042643	1268285	191.533	4.445	209	19	0.023603	0.0247357	0.86	14.628	0.034	46	34.7
J124645+055723	43106	191.688	5.956	119	15	0.0027919	0.0038937	11.75	13.269	0.028	39	31.6
J124701-013444	43128	191.754	-1.579	152	16	0.0090863	0.0102199	2.86	14.364	0.032	46	33.1
J124717+002405	43153	191.821	.401	136	19	0.0464121	0.0475821	0.6	15.553	0.08	62	33.09
J124727+030218	5093000	191.863	3.038	119	19	0.0175221	0.0186508	1.25	11.858	0.023	63	28.73
J124742+035222	43185	191.925	3.873	385	19	0.0338301	0.034973	2.79	12.534	0.026	58	34.47
J124753-011107	43198	191.971	-1.185	328	17	0.0234429	0.0245899	4.11	12.734	0.026	58	33.97
J124800+042609	3994854	192.000	4.436	129	19	0.0034024	0.0045087	1.41	14.431	0.035	40	32.95
J124813-032006	3105864	192.054	-3.335	99	18	0.0037659	0.0048941	5.34	10.011	0.02	66	25.97
J124903-011941	1121350	192.262	-1.328	102	18	0.0792148	0.0804219	0.67	13.696	0.028	40	31.44
J125038+012749	43470	192.658	1.464	173	15	0.0042429	0.0053552	2.65	12.828	0.025	66	31.11

